Article

Tumor suppressor PNRC1 blocks rRNA maturation by recruiting the decapping complex to the nucleolus

Marco Gaviraghi[1] (ID), Claudia Vivori[1,†], Yerma Pareja Sanchez[2], Francesca Invernizzi[3], Angela Cattaneo[4], Benedetta Maria Santoliquido[1], Michela Frenquelli[1], Simona Segalla[1], Angela Bachi[4], Claudio Doglioni[3], Vicent Pelechano[2], Davide Cittaro[5] & Giovanni Tonon[1,5,*] (ID)

Abstract

Focal deletions occur frequently in the cancer genome. However, the putative tumor-suppressive genes residing within these regions have been difficult to pinpoint. To robustly identify these genes, we implemented a computational approach based on non-negative matrix factorization, NMF, and interrogated the TCGA dataset. This analysis revealed a metagene signature including a small subset of genes showing pervasive hemizygous deletions, reduced expression in cancer patient samples, and nucleolar function. Amid the genes belonging to this signature, we have identified PNRC1, a nuclear receptor coactivator. We found that PNRC1 interacts with the cytoplasmic DCP1α/DCP2 decapping machinery and hauls it inside the nucleolus. PNRC1-dependent nucleolar translocation of the decapping complex is associated with a decrease in the 5′-capped U3 and U8 snoRNA fractions, hampering ribosomal RNA maturation. As a result, PNRC1 ablates the enhanced proliferation triggered by established oncogenes such as RAS and MYC. These observations uncover a previously undescribed mechanism of tumor suppression, whereby the cytoplasmic decapping machinery is hauled within nucleoli, tightly regulating ribosomal RNA maturation.

Introduction

The cancer genome is extensively rearranged, harboring somatic point mutations, chromosomal translocations as well as focal and large copy number alterations (CNAs). While there is overwhelming evidence that genes mutated or involved in chromosomal translocations exert crucial roles in carcinogenesis, the putative tumorigenic role of genes residing within gained or lost regions remains often elusive. In particular, identifying *bona fine* tumor suppressor genes (TSGs) within regions of chromosomal losses remains a daunting challenge. Building upon a survey that has collected genetic losses frequently present throughout various cancer types (Beroukhim *et al*, 2010), complementary approaches combining RNAi screens with sequencing-based information have led to the identification of novel TSGs (Nijhawan *et al*, 2012; Solimini *et al*, 2012). In particular, Solimini *et al* (2012) have revealed that within recurrent hemizygous focal deletions there is an enrichment of so-called STOP genes, which negatively affect proliferation. These studies have uncovered several unexpected TSGs that have been subsequently validated in depth (Solimini *et al*, 2013). However, a potential limitation of these approaches rests on the potential lack of cellular context (Goff, 2008; Mullenders & Bernards, 2009). Indeed, to vouch for consistency across experiments, oftentimes a single or, at most, a few reliable cell lines are used in these screens. As such, the appropriate biochemical and genetic environment might be missing, for cancer genes to unleash their oncogenic potential (Goff, 2008; Mullenders & Bernards, 2009). Furthermore, genes required for cancer cell survival *in vivo* are non-overlapping with those required *in vitro* (Miller *et al*, 2017). Hence, the exploitation of more extensive genomic data, including transcriptomic data, is warranted, for a more extensive and robust identification of potential TSGs.

1 Functional Genomics of Cancer Unit, Division of Experimental Oncology, Istituto di Ricovero e Cura a Carattere Scientifico (IRCCS) San Raffaele Scientific Institute, Milan, Italy
2 Science for Life Laboratory, Department of Microbiology, Tumor and Cell Biology, Karolinska Institutet, Solna, Sweden
3 Pathology Unit, Istituto di Ricovero e Cura a Carattere Scientifico (IRCCS) San Raffaele Scientific Institute, Milan, Italy
4 Functional Proteomics Program, Istituto FIRC di Oncologia Molecolare (IFOM), Milan, Italy
5 Center for Translational Genomics and Bioinformatics, Istituto di Ricovero e Cura a Carattere Scientifico (IRCCS) San Raffaele Scientific Institute, Milan, Italy
   *Corresponding author. Tel: +39 0226435624; E-mail: tonon.giovanni@hsr.it
   †Present address: Centre for Genomic Regulation (CRG), The Barcelona Institute for Science and Technology, Barcelona, Spain

Nucleoli are highly dynamic structures where ribosomal RNA (rRNA) is synthesized and processed. rRNA originates from specific DNA sequences called nucleolar organizer regions (NORs) spread along the short arms of all human acrocentric chromosomes (Babu & Verma, 1985). NORs contain several copies of tandem-repeated sequences of ribosomal DNA genes (rDNA) (Sylvester *et al*, 2004), which are extensively transcribed by RNA polymerase I (PolI) as long polycistronic RNA molecules containing three of the four mature rRNA species, separated by spacer sequences (Cui & Tseng, 2004). These long rRNA precursors are then extensively processed to release the mature 28S, 18S, and 5.8S rRNA isoforms, reviewed in Mullineux and Lafontaine (2012). Several classes of enzymes participate to this complex series of reactions, including RNA helicases, endonucleases, and exonucleases belonging both to the 5–3′ or 3′–5′ RNA-degrading pathways (Mullineux & Lafontaine, 2012; Preti *et al*, 2013; Sloan *et al*, 2013). In addition, a class of non-coding nucleolar RNAs called small nucleolar RNAs (snoRNAs) exerts a crucial role in rRNA maturation, mainly driving the editing of rRNA precursor molecules (Matera *et al*, 2007; Kiss *et al*, 2010). Of note, a subgroup of 5′-capped snoRNAs, including U3 and U8, promotes specific cleavage steps of pre-rRNA molecules, directly influencing rRNA processing rates (Peculis & Steitz, 1993; Fayet-Lebaron *et al*, 2009; Perez-Fernandez *et al*, 2011).

The size and number of nucleoli vary according to the rate of rRNA biosynthesis, which is carefully regulated according to various stimuli and stresses, and are frequently altered in different diseases (Boisvert *et al*, 2007) including cancer (Pianese, 1896). Indeed, aggressive tumors present hyperactivated rDNA transcription, which is required to boost ribosome biogenesis (Hein *et al*, 2013). Intriguingly, it is becoming evident that the increase in rRNA biogenesis triggered by oncogenic pathways is causally linked to cancer development (Barna *et al*, 2008; Chan *et al*, 2011). On the overall, the most established oncogenes, as, for example, MYC, RAS, and PI3K, strongly accelerate ribosome assembly by acting at the level of rRNA transcription and translation of ribosomal proteins (Boon *et al*, 2001; Arabi *et al*, 2003; Gomez-Roman *et al*, 2003; Schlosser *et al*, 2003; Zhao *et al*, 2003; Grandori *et al*, 2005; Mayer & Grummt, 2006; Drygin *et al*, 2010).

While the general roles of oncogenic pathways in promoting rRNA transcription have been defined, the mechanistic wiring underlying rRNA maturation remains largely unknown. Within this frame, we have identified a novel tumor suppressor gene, the proline-rich nuclear receptor coactivator 1 (PNRC1), as a novel regulator of rRNA maturation. PNRC1 is formally labeled as a nuclear receptor (NR) co-activator as it interacts with several NRs and trans-activates exogenous NR reporter targets in a ligand-dependent manner (Zhou *et al*, 2000). In addition, PNRC1 has been proposed as a negative regulator of the cytoplasmic RAS signaling pathway (Zhou *et al*, 2004). A putative role for PNRC1 in promoting rRNA transcription was inferred from its nucleolar localization and its interaction with NPM1 nucleolar protein (Wang *et al*, 2011), as well as from its ability to interact with a subunit of RNA polymerase III (Zhou *et al*, 2007). PNRC1 also interacts with the RNA helicase UPF1, even though PNRC1 downregulation does not interfere with the RNA decay processes controlled by UPF1 (Cho *et al*, 2009).

In this study, we show that PNRC1 re-expression in cancer cells interferes with rRNA processing through a novel molecular mechanism that relies on the nucleolar activity of the cytoplasmic DCP1α/DCP2 decapping complex, ultimately blocking oncogene-driven proliferation.

Results

Genes associated with the nucleolus are pervasively deleted and downregulated in several cancer types

Seeking to identify novel TSGs, we combined RNA-seq with copy number alterations (CNAs) data derived from 28 TCGA cancers, for which both datasets were available. As in previous genetic screen efforts (Nijhawan *et al*, 2012; Solimini *et al*, 2012), we focused on 82 focal deletion peaks reported as frequently lost in cancers of various origins. These regions harbor a total of 2,060 genes (Beroukhim *et al*, 2010). We applied a novel iteration of non-negative matrix factorization (NMF) to extract tumor-specific signatures, subsequently analyzed to create a generalized set of signatures, to capture the mutual distribution of CNAs and variation of expression (Brunet *et al*, 2004; Carrasco *et al*, 2006; Fig EV1A). One signature stood out, whereby concomitant copy number loss and gene expression reduction were evident (Fig 1A). Unlike the other signatures, where residing genes presented also instances of increased expression, the 158 genes underlying this cluster were consistently downregulated, across several cancer types (Appendix Table S1). Moreover, these genes were included in regions of the genome presenting mostly hemizygous deletions. We next asked whether these genes presented any shared biological feature. Analysis of Cellular Compartment annotation revealed that the nucleolus was the GO term most significantly associated with this signature. Mindful that gene annotations are often outdated (Riba *et al*, 2016; Wadi *et al*, 2016), we sought evidences from the literature associating the nucleolus with the list of STOP genes included in this cluster. Of note, we found that among the genes belonging to this cluster, four were both STOP and implicated with the nucleolus, namely TP53, SMAD4, HMGN1, and PNRC1.

In all, these observations reveal that a subset of putative TSGs resides within regions of hemizygous deletions, is consistently downregulated throughout tumor samples and is enriched for features associated with nucleolar activities.

PNRC1 loss is a frequent event in a wide variety of cancer types

While the nucleolar and cancer roles for TP53, SMAD4, and HMGN1 are established, PNRC1 is deemed a nuclear receptor coactivator, with only one report suggesting a nucleolar localization (Wang *et al*, 2011). PNRC1 resides within a region that is pervasively lost in a large arrays of tumors, including prostate cancer (Verhagen *et al*, 2002; Lapointe *et al*, 2007; Boyd *et al*, 2012; Kluth *et al*, 2013), pancreatic cancer (Johansson *et al*, 1992), breast cancer (Poplawski *et al*, 2010), T-cell neoplasms (Remke *et al*, 2009; Lopez-Nieva *et al*, 2012), and hepatocellular carcinoma (Lee *et al*, 2008).

We thus decided to explore in detail the potential role of PNRC1 as a putative tumor suppressor gene, in relationship with the nucleolus. We first substantiated the data emerging from the NMF analysis by analyzing PNRC1 expression levels in matched and unmatched tumor and normal samples. In line with the NMF
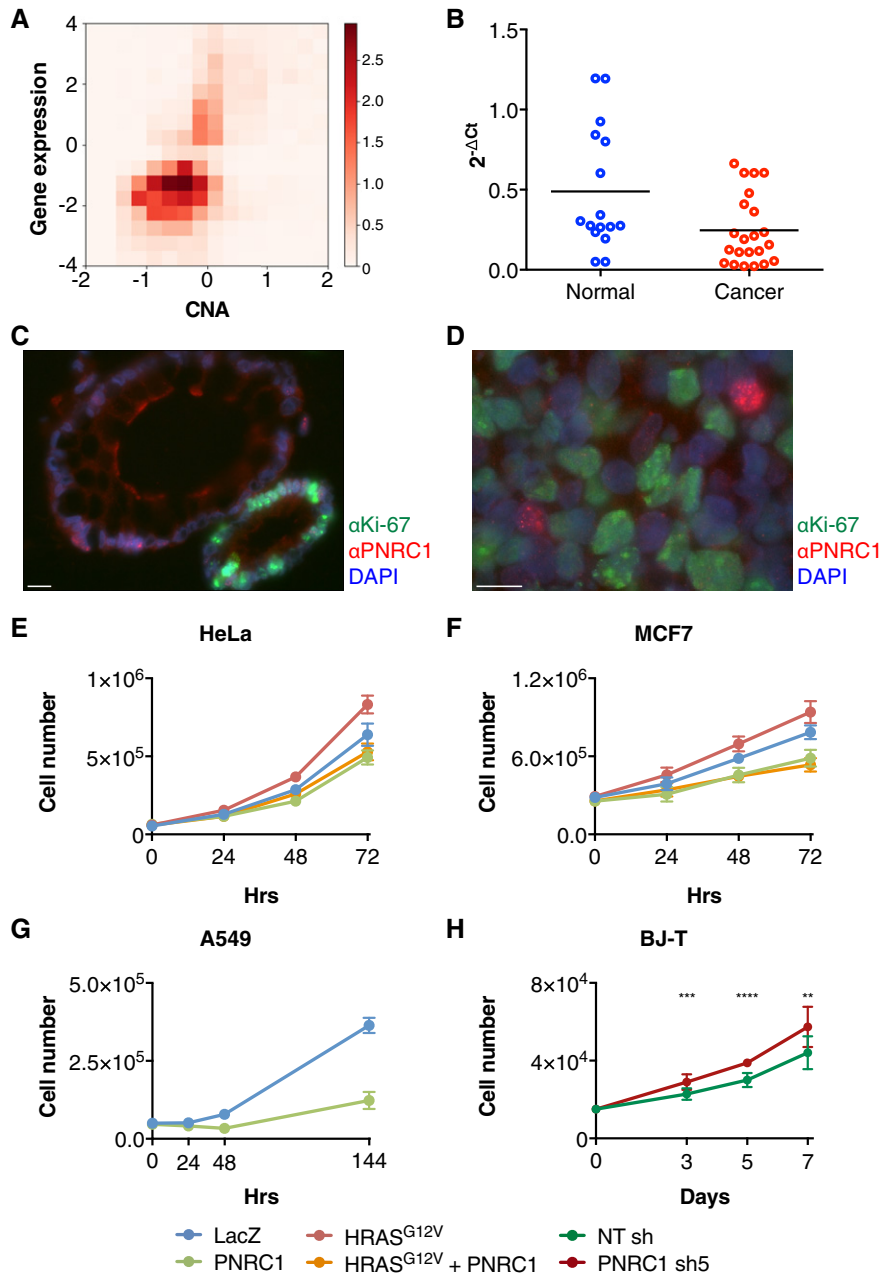
Figure 1. PNRC1 tumor suppressor hinders oncogene-induced hyperproliferation.

A   Visual representation of the signature found associated with hemizygously deleted and downregulated genes across multiple cancer types. The image represents the joint distribution of gene expression regulation (x-axis, z-score vs. normal tissue) and copy number alteration (CNA) (y-axis, exact segmentation value). Color intensity is proportional to the density value of the distribution.

B   Quantification of PNRC1 expression levels in primary normal (blue circles) and cancer (red circles) samples by real-time PCR.

C, D   Immunofluorescence staining of PNRC1 (red) and Ki-67 (green) performed on a primary healthy colon (C) or a malignant lymphoma (D). DAPI was used to stain cell nuclei. Scale bars: 50 μm.

E   Proliferation curves of HeLa cells transfected with HRAS^{G12V} (R), PNRC1 (P), their combination (RP), or a LacZ control (L). The results shown are the average ± SD of two biological replicates with three technical replicates each. A one-way ANOVA with Tukey multiple comparison test was performed for 72-h dataset; the statistically significant comparisons are: L vs. R ($P < 0.002$), L vs. P ($P < 0.02$), R vs. P ($P < 0.0002$), and R vs. RP ($P < 0.0004$).

F   Proliferation curves of MCF7 cells transfected with HRAS^{G12V} (R), PNRC1 (P), their combination (RP), or a LacZ control (L). The results shown are the average ± SD of two biological replicates with three technical replicates each. A one-way ANOVA with Tukey multiple comparison test was performed for 72-h dataset; the statistically significant comparisons are: L vs. R ($P < 0.003$), L vs. P ($P < 0.0002$), L vs. RP ($P < 0.0001$), R vs. P ($P < 0.0001$), and R vs. RP ($P < 0.0001$).

G   Proliferation curves of KRAS^{G12S}-mutated A549 cells transfected with PNRC1 or LacZ control. A representative experiment with the average ± SD of three technical replicates is shown. An unpaired t-test was performed for 144-h dataset ($P < 0.0003$).

H   Proliferation curves of BJ-T cells transduced with a non-targeting (NT sh) or a PNRC1-specific shRNA construct (PNRC1 sh5). Results are shown as the average ± SD of three biological replicates with three technical replicates each. An unpaired t-test was performed for each time point (**$P < 0.01$, ***$P < 0.005$, ****$P < 0.001$).

analysis of TCGA data, PNRC1 expression was consistently lower in cancer compared to normal tissues (Figs 1B and EV1B). We also explored PNRC1 expression by immunofluorescence. Remarkably, both in cancer and in healthy tissues, the distribution of PNRC1 and the distribution of a proliferation marker, Ki-67, were steadily mutually exclusive (Figs 1C and D, and EV1C and D), suggesting that PNRC1 expression is a feature of non-proliferative cells.

In all, these results suggest that PNRC1 might represent a novel tumor suppressor gene, based on its pervasive downregulation and localization within regions of hemizygous loss in cancer.

PNRC1 thwarts RAS and MYC-driven proliferation

As a first appraisal of the potential role of PNRC1 as a TSG, we tested whether PNRC1 could interfere with oncogene-induced enhanced proliferation in HeLa and MCF7 cell lines, which show low endogenous PNRC1 expression levels (Fig EV1B). The exogenous expression of PNRC1 by itself significantly reduced proliferation, when compared with the mock transfection, in HeLa (Fig 1E and Appendix Fig S1A) and MCF7 (Fig 1F and Appendix Fig S1B) cells in the absence of apoptosis (Fig EV2C), in line with a previous report (Zhou *et al*, 2004). To determine whether PNRC1 could impede oncogene-induced proliferation, we transfected PNRC1 alongside the HRAS^{G12V} oncogene. Remarkably, the increased proliferation following HRAS^{G12V} overexpression was completely ablated by the co-expression of PNRC1 in both cell lines (Fig 1E and F and Appendix Fig S2A). As a confirmation, PNRC1 expression reduced proliferation also of A549 cells, which endogenously express KRAS^{G12S} (Fig 1G and Appendix Fig S1C), as well as the anchorage-independent growth of HeLa (Fig EV2A) and A549 cells (Fig EV2B). We then explored whether the suppressive effect of PNRC1 on proliferation was more pervasive, extending also to other oncogenic pathways. We thus expressed PNRC1 alongside MYC in HeLa cells. As for HRAS^{G12V} overexpression, PNRC1 completely ablated MYC-induced proliferation (Fig EV1E and Appendix Fig S1D). To corroborate these results, we also silenced endogenous PNRC1 by shRNA. Whereas an almost complete PNRC1 silencing triggered apoptosis in HeLa cells (Fig EV2D and E, and Appendix Fig S2B), its mild downregulation resulted in an increased proliferative ability of immortalized BJ-T fibroblasts (Fig 1H and Appendix Fig S1E). Taken together, these data demonstrate that PNRC1 restrains the enhanced proliferation conferred by the expression of potent oncogenes and suggest that PNRC1 is endowed with tumor-suppressive activities.

PNRC1 affects nucleolar RNA dynamics

Since from the TCGA data PNRC1 belongs to a signature characterized by the nucleolus GO term, we next explored whether PNRC1 had any broad activity in the regulation of nucleolar RNA dynamics. To this end, we initially performed an unbiased experiment taking advantage of the Click-iT pulse-chase approach. We exogenously expressed an RFP-tagged form of PNRC1 or an RFP control in HeLa cells (Appendix Fig S2C) and we pulsed cells with 5-ethynyl uridine (EU) for 16 h. Cells were then chased and the intensity and localization of neo-transcribed RNAs were followed by confocal microscopy. In line with a previous work (Wang *et al*, 2011), we could observe the accumulation of RFP-PNRC1 fusion protein in nuclear structures resembling nucleoli. Moreover, whereas control

RFP-expressing cells showed an intense RNA signal inside nucleoli at earlier times, in RFP-PNRC1-transfected cells we could observe a dramatic reduction in the overall neotranscribed RNA, with a strong decrease in nascent RNA signal inside nucleoli (Fig 2A). In all, these results suggest that PNRC1 might negatively regulate rRNA biogenesis.

We next aimed to determine the molecular role of PNRC1 in the repression of rRNA synthesis. According to the literature, rRNA transcription occurs between the inner nucleolar fibrillar centers (FC) and the surrounding dense fibrillar component (DFC), where rDNA is complexed with UBF1 transcription factor and RNA PolI machinery (Raska, 2003; Moss *et al*, 2007). Once transcribed, rRNA is processed in a contiguous sub-nucleolar compartment, the outer granular component (GC), defined by the presence of nucleophosmin (NPM1) protein (Boisvert *et al*, 2007; Ma & Pederson, 2008). To initially define whether PNRC1 participates in rRNA transcription or in rRNA processing, we aimed to define PNRC1 sub-nucleolar localization in relationship with UBF1 and NPM1 nucleolar markers, respectively. As reported (Wang *et al*, 2011), HA-PNRC1 co-precipitated with NPM1 (Fig EV3A). In line with this observation, our confocal microscopy experiments showed a strict co-localization between GFP-PNRC1 and NPM1 (Fig 2B). Notably, however, GFP-PNRC1 localization was mutually exclusive with UBF1 (Fig 2C), indicating that PNRC1 resides exclusively within the nucleolar GC. These data hence suggest that PNRC1 does not participate in rRNA transcription, as previously proposed (Wang *et al*, 2011), but instead regulates rRNA processing.

To strengthen these observations, we performed a pulse-chase rRNA processing assay. HeLa cells transiently transfected with PNRC1 or a LacZ control (Appendix Fig S2D) were pulsed with ^{3}H-uridine for 15 min. RNA was then collected at different time points after the chase, was resolved onto a denaturing gel, blotted, and subjected to autoradiography. As a positive control, 5-fluorouridine (FU) was used, which blocks rRNA processing (Wilkinson *et al*, 1975). Upon PNRC1 expression, the levels of the mature 28S rRNA form decreased, as well as of its 32S precursor, while a transient accumulation of the 47S pre-rRNA was evident (Fig 2D). Accordingly, we observed an increase in the ratios between the 47S precursor and the 32S and 28S rRNA molecules in PNRC1-expressing cell lines compared to the control (Fig 2E). To corroborate these observations, we then measured the steady-state levels of the 47S pre-rRNA intermediate in HeLa cells expressing PNRC1 or GFP control (Appendix Fig S2E) by real-time PCR. In line with the pulse-chase experiments, PNRC1 expression led to a significant increase in both 5'-ETS (Fig 2F) and ITS1 (Fig EV3B) as a result of 47S pre-rRNA accumulation.

Taken together, these results indicate that PNRC1 inhibits rRNA processing, thus leading to the accumulation of unprocessed rRNA precursors and to a decrease in mature rRNA molecules.

PNRC1 interacts with the cytoplasmic RNA decapping machinery

PNRC1 presents several protein–protein interaction domains but lacks any intrinsic enzymatic activity. Therefore, we reasoned that PNRC1-mediated block of rRNA processing might result from the activity of its interacting proteins. To corroborate this hypothesis, we first sought to identify PNRC1 interactors by analyzing PNRC1 co-immunoprecipitating proteins by mass spectrometry in
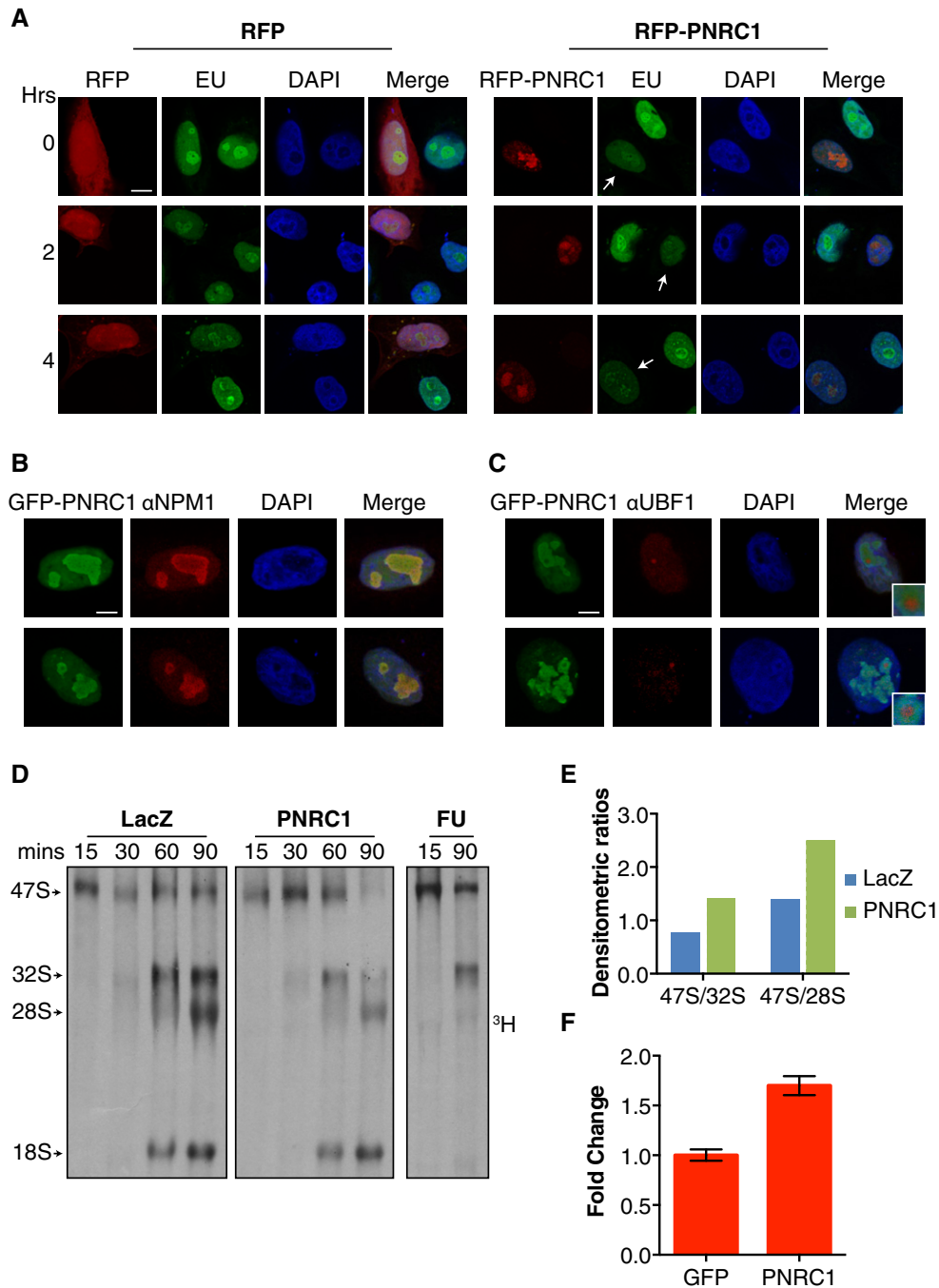
Figure 2. PNRC1 interferes with nucleolar RNA metabolism.

A   Click-iT RNA imaging assay performed on HeLa cells expressing RFP-PNRC1 or RFP control. Confocal images of transfected cells pulsed with EU for 16 h were collected at the indicated time points after EU removal (green: Alexa 488-EU, red: RFP, blue: DAPI, scale bar: 5 μm). RFP-PNRC1-transfected cells are indicated with arrowheads.

B, C   Confocal microscopy images of HeLa cells expressing GFP-PNRC1 and stained with antibodies against NPM1 (B) or UBF1 (C) nucleolar proteins (nuclei are stained in blue with DAPI, scale bar: 5 μm). Two representative cells are shown for each staining. A magnification of the merged channel images is provided for UBF1 staining.

D   Agarose/formaldehyde gel separation of neotranscribed rRNAs collected from LacZ and PNRC1-expressing cells pulsed for 15 min with ^{3}H-uridine and chased for the reported time points (minutes). Samples were loaded according to the amount of incorporated ^{3}H, quantified by liquid scintillation. 5-fluorouridine (FU) was included as a control of a blocked rRNA processing.

E   Ratios between the intensity of 47S pre-rRNA band and bands belonging to 32S or 28S rRNA species relative to panel (D) and measured at 60 min after the chase for both LacZ or PNRC1-expressing cells.

F   Real-time PCR quantification of 5′-ETS steady-state levels in HeLa cells expressing PNRC1 or GFP control. The average ± SD of three biological replicates is shown. Statistical significance was calculated by an unpaired two-tailed *t*-test (*P* < 0.0001).

PNRC1-expressing HeLa cells. As expected, we could observe a strong enrichment of PNRC1 protein by both Western blot and mass spectrometry analysis (Fig 3A and B, and Table 1). Intriguingly, we identified the regulatory RNA decapping protein DCP1α and the enhancer of decapping EDC3 as two of the most enriched PNRC1 co-immunoprecipitating proteins (Table 1). Moreover, other RNA decapping-related proteins were identified as specifically enriched in the PNRC1-IP fraction, including the RNA helicases DDX6 and UPF1 (Table 1 and Appendix Table S2), previously identified as a PNRC1-interacting protein (Cho *et al*, 2009). All these proteins are known to form a complex in the cytoplasm that promotes the removal of the 5′ m^{7}G cap from aberrant messenger RNAs, as part of the NMD pathway, reviewed in Parker and Sheth (2007).

Prompted by these results, we initially validated the hits identified by mass spectrometry by co-immunoprecipitation. Using an anti-HA antibody, we confirmed a strong enrichment of DCP1α among HA-PNRC1 co-immunoprecipitating proteins (Fig 3C). Notably, this interaction was maintained even upon treatment of cell lysates with RNase A, thus suggesting that it is not mediated by RNA molecules (Fig 3C and Appendix Fig S2F). This protein–protein interaction was further confirmed by a reverse DCP1α co-immunoprecipitation performed on PNRC1-expressing HeLa cells (Fig 3D) and by a PNRC1 co-immunoprecipitation performed on non-transfected HeLa cells (Fig 3E), suggesting that the endogenous PNRC1 can interact with DCP1α.

To assess whether PNRC1 could interact with the whole decapping machinery, we expanded our analysis to other members of the RNA decapping complex. Indeed, by immunoprecipitation, we were able to show that PNRC1 co-purifies with crucial players of the decapping machinery, including the catalytic RNA decapping subunit DCP2 and the DDX6 RNA helicase (Fig 3F and G).

Taken together, these results show that PNRC1 binds the cytoplasmic decapping machinery and suggest that PNRC1 might play a role in regulating RNA decapping dynamics.

PNRC1 recruits the RNA decapping machinery inside nucleoli

Our data imply that PNRC1 is exclusively nuclear, mainly localized in the nucleolar GC. Conversely, the DCP1α/DCP2 decapping complex has been reported as cytoplasmic, acting in specialized structures called processing bodies (P-bodies). There, the DCP1α/DCP2 decapping machinery accumulates alongside RNA-degrading enzymes and their substrate RNAs (Parker & Sheth, 2007). To clarify the reciprocal localization of PNRC1 and the DCP1α/DCP2 decapping complex, we initially studied whether PNRC1 may impact on the subcellular distribution of P-bodies protein. To this end, we performed immunofluorescence staining for the decapping complex proteins DCP1α, DDX6, or LSM1 in HeLa cells expressing RFP-PNRC1 or RFP control. We then counted the cells according to the presence of these markers inside P-bodies. As shown in Fig 4A and B, in the vast majority of RFP-expressing cells DCP1α, DDX6 and LSM1 proteins localized in sharp cytoplasmic dots corresponding to P-bodies. On the contrary, we could observe a complete loss of the P-body localization of these three markers in almost every RFP-PNRC1-transfected cell. This result indicates that PNRC1 expression alters the canonical cytoplasmic localization of P-bodies proteins.

We then reasoned that PNRC1 interaction with the decapping machinery might promote its re-localization inside nucleoli. To explore this hypothesis, we evaluated whether PNRC1 expression could drive DCP1α re-localization by a biochemical cell fractionation assay (Fig 4C). Strikingly, upon PNRC1 expression, we could
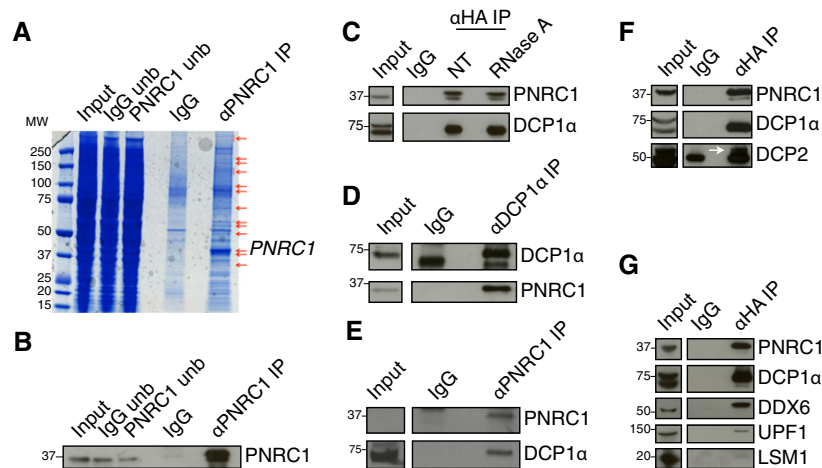

Figure 3.   **PNRC1 interacts with cytoplasmic RNA decapping proteins.**

A, B   Coomassie blue staining and Western blot analysis of the SDS–PAGE gel corresponding to PNRC1 immunoprecipitation. Red arrows represent the gel areas excised both from the IgG and IP lanes for mass spectrometry analysis. Input, unbound, and IP fractions were loaded as reported. The protein band corresponding to PNRC1 is indicated.

C   Co-immunoprecipitation performed on HeLa cells expressing HA-PNRC1 with a specific anti-HA antibody in absence or presence of 1 mg/ml RNaseA.

D   Co-immunoprecipitation of DCP1α-interacting proteins performed on HA-PNRC1-expressing HeLa cells with a specific anti-DCP1α antibody.

E   Co-immunoprecipitation performed on wild-type HeLa cells with an anti-PNRC1 antibody and probed for DCP1α.

F, G   Co-immunoprecipitation performed on HeLa cells expressing HA-PNRC1 with a specific anti-HA antibody and probed with antibodies specific for proteins involved in RNA decapping. The white arrow indicates the specific DCP2 band, as reported in the datasheet of the antibody employed.

Source data are available online for this figure.

Table 1. Highest enriched proteins obtained by mass spectrometry.

Protein name	UniProt ID	MW (kDa)	IgG peptides	IP peptides
Proline-rich nuclear receptor coactivator 1 OS = *Homo sapiens* GN = PNRC1	Q12796	35	11	27
mRNA-decapping enzyme 1A OS = *Homo sapiens* GN = DCP1A	Q9NPI6	63	0	21
Enhancer of mRNA-decapping protein 3 OS = *Homo sapiens* GN = EDC3	Q96F86	56	0	21
Regulator of nonsense transcripts 1 OS = *Homo sapiens* GN = UPF1	Q92900	124	2	10
Enhancer of mRNA-decapping protein 4 OS = *Homo sapiens* GN = EDC4	Q6P2E9	152	0	4
Probable ATP-dependent RNA helicase DDX6 OS = *Homo sapiens* GN = DDX6	P26196	54	0	8

appreciate a remarkable enrichment of DCP1α in the nucleolar fraction, confirming that PNRC1 interacts with DCP1α in this cellular compartment (Fig 4C and D). To corroborate these data, we co-expressed a shRNA-resistant GFP-DCP1α in combination with RFP-PNRC1 or RFP control in HeLa cells knocked-down for endogenous DCP1α (Appendix Fig S3A). As expected, GFP-DCP1α accumulated inside P-bodies in RFP control-expressing cells while it co-localized with RFP-PNRC1 inside nucleoli upon the expression of RFP-PNRC1 fusion protein (Fig 4E). Moreover, after pre-permeabilizing cells with CSK buffer supplemented with RNase A, immunofluorescence experiments revealed that endogenous DCP1α co-localizes with RFP-PNRC1 and NPM1 while it is excluded from nucleoli in control RFP-expressing cells (Fig EV3C).

In all, these data show that PNRC1 interaction with the RNA decapping machinery elicits its translocation inside nucleoli.

W300A mutation impairs PNRC1 interaction with DCP1α/DCP2 molecular machinery and its nucleolar recruitment

To determine whether the nucleolar interaction between PNRC1 and DCP1α/DCP2 is required for the PNRC1-dependent block in rRNA biogenesis, we sought to generate a PNRC1 mutant form unable to bind to the decapping machinery. The PNRC1 paralog PNRC2 resides in the cytoplasm where it interacts with DCP1α inside P-bodies (Cho *et al*, 2009, 2012, 2015). PNRC2 P108 and W114 residues are mainly responsible for PNRC2 binding to DCP1α, as alanine substitutions of each of these amino acids (in particular W114A) prevent PNRC2-DCP1α interaction (Lai *et al*, 2012). Notably, both these residues lie in a region that is exceedingly conserved between PNRC2 and PNRC1. We thus reasoned that

mutations on these residues might be crucial to mediate the interaction between PNRC1 and DCP1α. We hence mutagenized PNRC1 W300 residue, corresponding to W114 on PNRC2, into an alanine. Of note, PNRC1^{W300A} did not show any evident reduction in protein stability and localized inside nucleoli as the wild-type isoform (Fig EV4A and Appendix Fig S3B). We then explored the effects of W300A mutation on the binding between PNRC1 and its interacting partners. As control, we generated HA-PNRC1$^{\Delta NLS}$ mutant by deleting the NLS/NoLS sequence that grants PNRC1 nucleolar localization through its interaction with NPM1 (Wang *et al*, 2011). We observed that W300A mutation almost completely abolished PNRC1 ability to co-purify with DCP1α, while maintained its ability to interact with NPM1 (Fig 5A) and localize to the nucleolus (Fig EV4A). Conversely, PNRC1$^{\Delta NLS}$ mutant did not interact with NPM1 but intriguingly maintained the binding to DCP1α. We then broadened our analysis to other members of the decapping complex. To this end, HeLa cells were transfected with HA-tagged forms of PNRC1^{W300A} and co-immunoprecipitation using an anti-HA antibody was performed. PNRC1^{W300A} mutant did not co-purify with both DCP1α and DCP2 decapping proteins, as well as with DDX6 RNA helicase (Fig 5B and C). Altogether, these results indicate that the W300A substitution abolishes the ability of PNRC1 to interact with the decapping machinery.

To determine whether PNRC1^{W300A} was still able to re-localize the decapping machinery to the nucleolus, we performed confocal microscopy experiments by expressing the sh-resistant form of GFP-DCP1α in combination with RFP-PNRC1^{WT}, RFP-PNRC1^{W300A}, or RFP control transgenes in HeLa cells silenced for endogenous DCP1α (Appendix Fig S3A). Whereas RFP-PNRC1^{W300A} showed the same nucleolar localization of RFP-PNRC1^{WT}, we could not detect any co-localization of GFP-DCP1α with RFP-PNRC1^{W300A} inside nucleoli. Indeed, GFP-DCP1α localized in the nucleolus only when co-expressed with RFP-PNRC1^{WT}, while it remained almost completely embedded in cytoplasmic P-bodies in the presence of RFP-PNRC1^{W300A} (Fig 5D). In line with these results, immunofluorescence experiments on pre-permeabilized cells showed that endogenous DCP1α does not localize inside nucleoli in RFP-PNRC1^{W300A}-expressing cells (Fig EV3C). Moreover, the expression of RFP-PNRC1^{W300A} did not interfere with the cytoplasmic localization of DCP1α, DDX6, and LSM1, as shown by immunofluorescence experiments (Fig 5E and F). Specifically, whereas almost every cell expressing RFP-PNRC1^{WT} was devoid of P-bodies (Figs 4A and B, and 5E central panel), the three markers localized in the P-bodies in about 60% of RFP-PNRC1^{W300A}-transfected cells (Fig 5E and F). These results suggest that the W300A mutation on PNRC1 impedes the re-localization of the decapping machinery inside the nucleolus.

To conclusively demonstrate that PNRC1 is required for this re-localization, we evaluated whether DCP1α could complex with NPM1 in presence of PNRC1^{WT}, PNRC1^{W300A}, or PNRC1$^{\Delta NLS}$ mutants by performing a co-immunoprecipitation experiment with an anti-DCP1α antibody. As shown in Fig 5G, we observed that DCP1α interacted with NPM1 only in cells expressing HA-PNRC1^{WT}. Indeed, both W300A mutation and NLS deletion in PNRC1 impaired DCP1α-NPM1 interaction. These data thus demonstrate that DCP1α can indirectly interact with NPM1, and this interaction is mediated by PNRC1^{WT}.

Taken together, these results indicate that the recruitment of DCP1α/DCP2 decapping machinery to the nucleolus is a direct consequence of DCP1α-PNRC1 binding and suggest that PNRC1
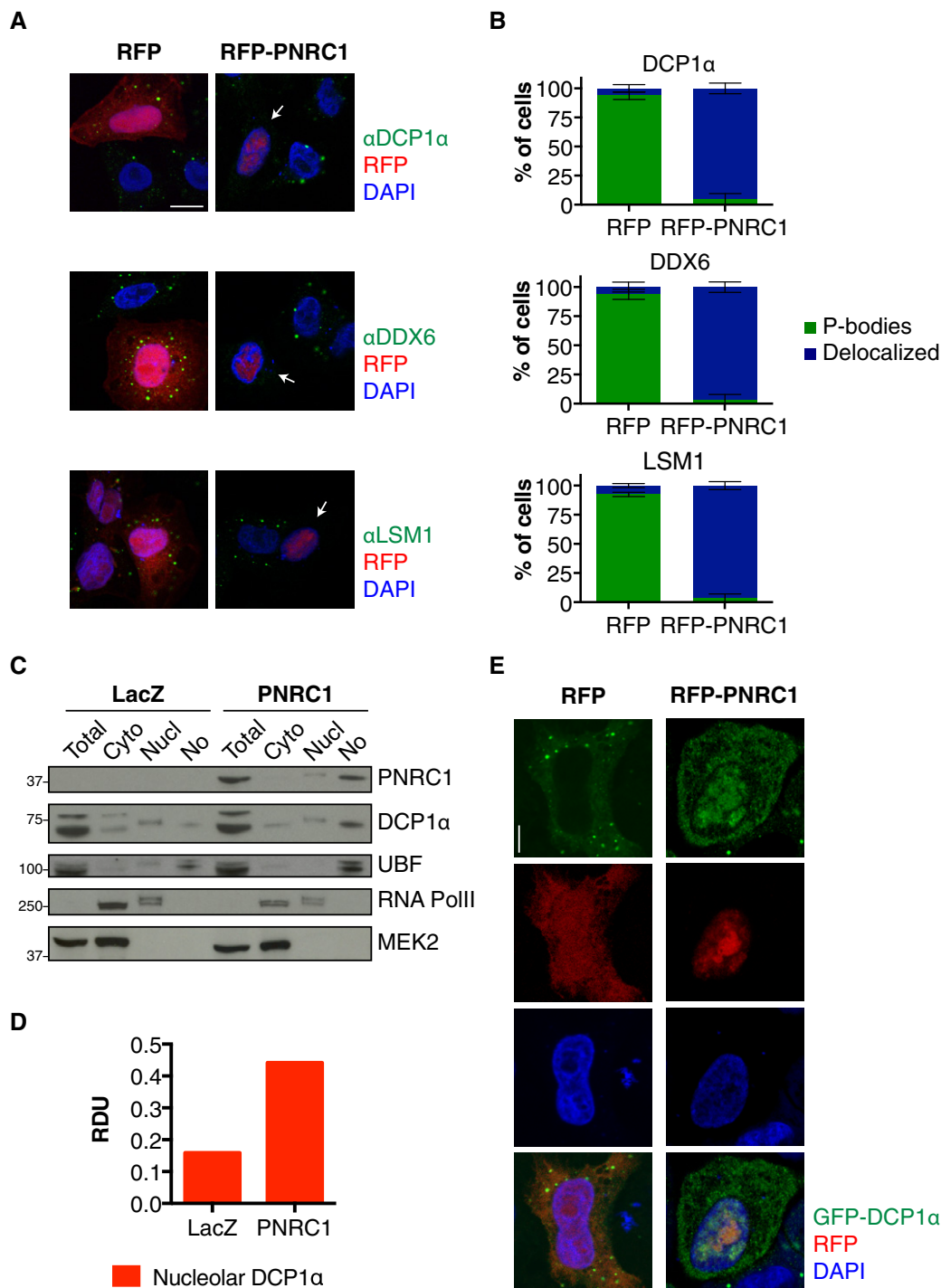
Figure 4. Re-localization of the RNA decapping machinery upon PNRC1 expression.

A   Confocal microscopy images of RFP or RFP-PNRC1-expressing cells stained for DCP1α, DDX6, and LSM1. RFP-PNRC1-transfected cells are indicated with arrowheads. Scale bar: 10 μm.

B   Quantification of cells classified according to the P-body localization of the three stained proteins. The average ± SD of three independent experiments is reported.

C   Nucleolar fractionation performed on LacZ- or PNRC1-expressing HeLa cells. Total lysates, cytoplasmic (Cyto), nucleoplasmic (Nucl), and nucleolar (No) fractions were collected. UBF1, RNA PolII, and MEK2 were used as markers for the nucleolar, non-nucleolar and cytoplasmic fractions, respectively. The electrophoretic mobility of proteins in the nucleoplasmic lanes is slightly diminished due to nuclear lysis buffer composition.

D   Densitometric quantification of DCP1α nucleolar pool obtained from the Western blot shown in panel (C) and normalized upon the amount of nucleolar UBF1 and the levels of DCP1α in the input fraction.

E   Confocal microscopy images of HeLa cells silenced for the endogenous DCP1α and expressing a shRNA-resistant GFP-DCP1α in combination with RFP or RFP-PNRC1 transgenes (green: GFP, red: RFP, blue: DAPI, scale bar: 5 μm).
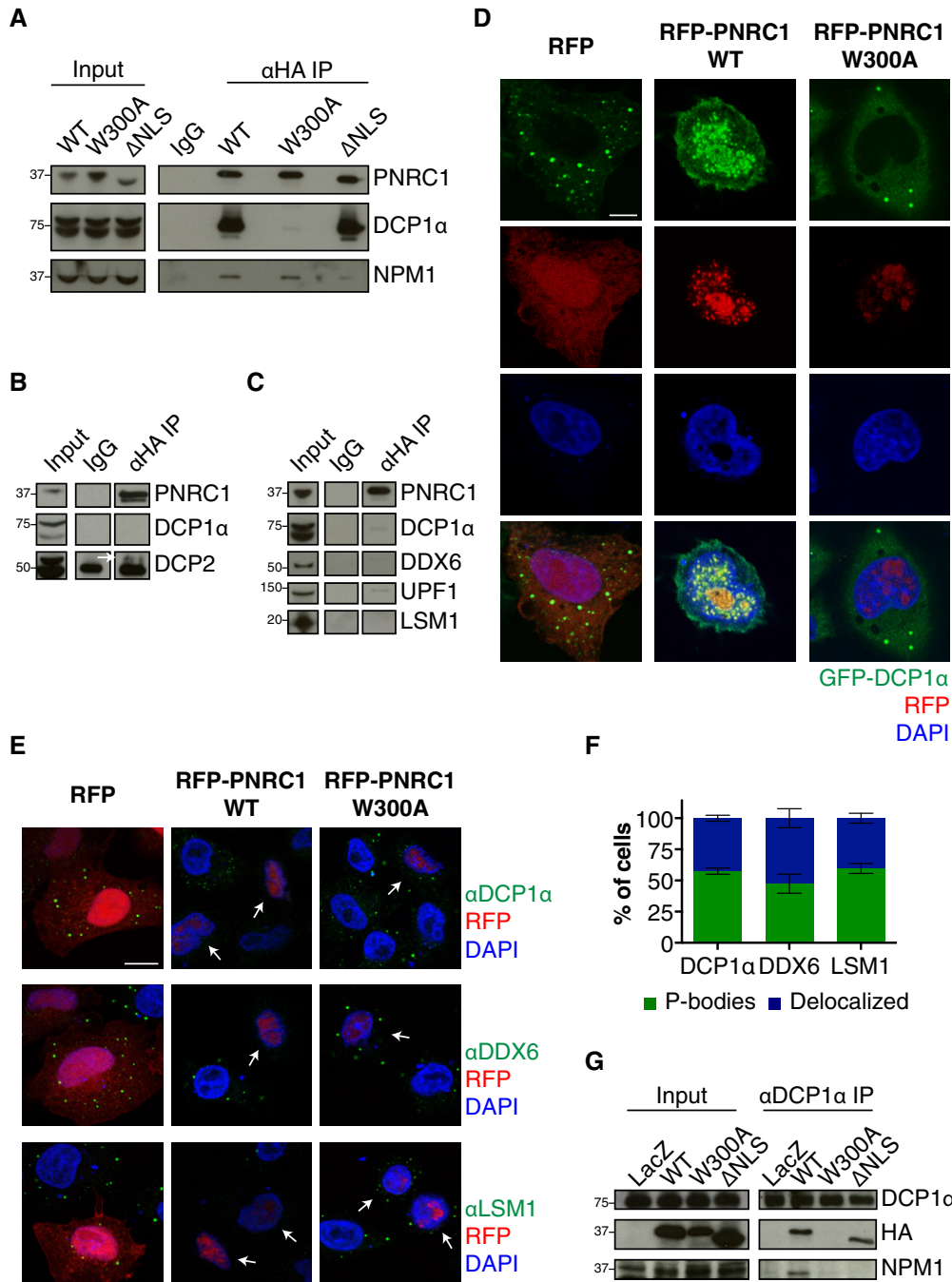
Figure 5. W300A mutation impairs PNRC1 interaction with DCP1α and its nucleolar translocation.

A   Co-immunoprecipitation performed on HeLa cells expressing HA-PNRC1^{WT}, HA-PNRC1^{W300A}, or HA-PNRC1$^{\Delta NLS}$ with a specific anti-HA antibody and probed with anti-NPM1 and anti-DCP1α antibodies.

B, C   Co-immunoprecipitation performed on HeLa cells expressing HA-PNRC1^{W300A} mutant with a specific anti-HA antibody and probed with antibodies specific for PNRC1-interacting proteins. The white arrow indicates the specific DCP2 band.

D   Confocal microscopy images of HeLa cells silenced for the endogenous DCP1α and expressing an shRNA-resistant GFP-DCP1α in combination with RFP, RFP-PNRC1^{WT}, or RFP-PNRC1^{W300A} mutant (green: GFP, red: RFP, blue: DAPI, scale bar: 5 μm).

E   Confocal microscopy images of RFP-, RFP-PNRC1-, or RFP-PNRC1^{W300A}-expressing cells stained for DCP1α, DDX6, and LSM1. RFP-PNRC1^{WT}- or RFP-PNRC1^{W300A}-transfected cells are indicated with arrowheads. Scale bar: 10 μm.

F   Quantification of HeLa cells expressing RFP-PNRC1^{W300A} classified according to the P-body localization of the three stained proteins. The average of three independent experiments ± SD is reported.

G   Co-immunoprecipitation performed on HeLa cells expressing LacZ control, HA-PNRC1^{WT}, HA-PNRC1^{W300A}, or HA-PNRC1$^{\Delta NLS}$ constructs with a specific anti-DCP1α antibody and probed with anti-PNRC1 and anti-NPM1 antibodies.

Source data are available online for this figure.

promotes the localization of the decapping complex to nucleoli bridging DCP1α and NPM1 proteins.

The DCP1α/DCP2 decapping complex re-localization to the nucleolus modulates rRNA processing

We next explored the role of the nucleolar DCP1α/DCP2 complex in modulating rRNA dynamics. To this end, we performed a Click-iT pulse-chase assay on HeLa cells expressing RFP-tagged fusions of PNRC1^{WT}, PNRC1^{W300A} or RFP control (Appendix Fig S3B). While RFP-PNRC1^{WT} expression deeply reduced nascent nucleolar RNA signal, RFP-PNRC1^{W300A}, as RFP control, did not exert any effect, suggesting that PNRC1^{W300A} does not significantly alter nascent rRNA biogenesis (Fig 6A). To corroborate these results, we evaluated the steady-state levels of 47S pre-rRNA in PNRC1^{W300A}-expressing cells (Appendix Fig S3C) as a readout of rRNA processing block. Unlike PNRC1^{WT} (Fig 2F), PNRC1^{W300A} did not induce any accumulation of the 47S polycistronic rRNA molecule, as shown by the real-time PCR quantification of 5′-ETS and ITS1 sequences (Figs 6B and EV4B).

In all, these data indicate that the PNRC1-mediated re-localization of the decapping complex inside nucleoli is responsible to restrain rRNA biogenesis.

DCP2 catalytic subunit is required to promote PNRC1-dependent block in rRNA processing

To conclusively prove that the rRNA processing block mediated by PNRC1 relies on the decapping activity of the DCP1α/DCP2 complex, we evaluated whether the silencing of DCP2 catalytic subunit could prevent the PNRC1-triggered accumulation of 47S pre-rRNA molecule. To this end, we knocked-down DCP2 in HeLa cells with a specific shRNA construct. DCP2-silenced cells were further infected with GFP control, PNRC1^{WT}, or PNRC1^{W300A} transgenes (Appendix Fig S3D) and the steady-state levels of 5′-ETS were measured by real-time PCR. In agreement with our previous results, HeLa cells infected with a non-targeting shRNA displayed a significant increase in 5′-ETS levels following PNRC1^{WT} expression that was almost completely blunted in PNRC1^{W300A}-expressing cells (Fig 6C). Intriguingly, DCP2 silencing ablated the increase in 5′-ETS levels elicited by PNRC1^{WT}, suggesting that DCP2 is essential in inducing PNRC1-dependent accumulation of rRNA precursors.

Nucleolar DCP1α/DCP2 complex is associated with the decapping of U3 and U8 snoRNAs

We have shown that PNRC1-dependent block in rRNA processing is dependent on the activity of the DCP1α/DCP2 decapping machinery inside nucleoli. However, rRNA species do not harbor cap structures at their 5′ ends. We then hypothesized that the PNRC1-orchestrated nucleolar decapping complex might indirectly block rRNA processing by promoting the decapping of other nucleolar RNAs that in turn regulate rRNA maturation dynamics. Along this line, the early cleavage steps of the 47S pre-rRNA transcript require the base pairing of U3 and U8 snoRNAs to sequences contained respectively in the 5′-ETS region of the 47S rRNA precursor and in the 5′ portion of the maturing 28S rRNA (Peculis & Steitz, 1993; Peculis, 1997; Marmier-Gourrier *et al*, 2011; Mullineux & Lafontaine, 2012). Interestingly, both U3 and U8 snoRNAs are transcribed by RNA polymerase II and

receive a mono-methylated (m^{7}G) 5′ cap that is further converted into a tri-methylated cap structure (m$_3$G) during their maturation (Peculis & Steitz, 1994; Verheggen *et al*, 2002; Matera *et al*, 2007). Stemming from these evidences, we assayed whether U3 and U8 could represent potential targets for the nucleolar DCP1α/DCP2 decapping machinery. To this end, we collected total RNA from HeLa cells expressing PNRC1^{WT}, PNRC1^{W300A}, or a GFP control and we immunoprecipitated RNAs harboring a tri-methylated 5′ cap with an anti-m$_3$G cap antibody. We then measured the abundance of total or immunoprecipitated U3 and U8 in the different conditions by real-time PCR. Whereas we could not detect significant changes in the expression levels of both snoRNAs between the three conditions assayed (Fig EV4C), we observed a remarkable decrease in the immunoprecipitated U3 and U8 in PNRC1^{WT}-expressing cells, partially recovered in cells expressing PNRC1^{W300A} (Fig 6D and E). As a control, we did not observe any significant differences among the three conditions in the amount of the immunoprecipitated U1 small nuclear RNA (snRNA) that, like U3 and U8, is endowed with a 5′ m$_3$G cap (Fig EV4D).

To further corroborate these results, we analyzed the capping status of these RNAs taking advantage of a linker ligation assay by ligating a specific 5′ linker (5LINK) to uncapped RNA molecules. In line with m$_3$G-cap IP results, the levels of ligated U3 and U8 snoRNAs, but not of U1 snRNA, increased specifically in PNRC1^{WT}-expressing cells compared to PNRC1^{W300A} or GFP control conditions (Fig EV4E).

Finally, to assess whether DCP2 is directly responsible for PNRC1-mediated snoRNA decapping, we immunoprecipitated m$_3$G RNAs in cells silenced for DCP2 and expressing GFP control, PNRC1^{WT}, or PNRC1^{W300A} transgenes (Appendix Fig S3D) and we observed that DCP2 silencing prevented the reduction in the levels of immunoprecipitated U3 observed in PNRC1^{WT}-expressing cells (Fig 6F).

Taken together, these data indicate that the PNRC1-recruited nucleolar DCP1α/DCP2 complex is likely responsible for U3 and U8 snoRNA decapping, ultimately blocking rRNA processing.

PNRC1 binds to U3 and U8 snoRNAs

Our data show that PNRC1 function relies on its ability to bind DCP1α/DCP2 decapping machinery inside nucleoli. We next asked whether PNRC1 could also bind its substrate RNAs. To this end, we performed an RNA immunoprecipitation (RIP) in HeLa cells by precipitating Flag-tagged GFP, PNRC1^{WT}, or PNRC1^{W300A} with anti-Flag-coated beads (Fig 6G). Strikingly, we observed a significant increase in U3 and U8 snoRNAs co-precipitating with PNRC1^{WT} compared to GFP control, but not of the U1 snRNA (Fig 6H). Intriguingly, the levels of co-precipitated snoRNAs were similar between PNRC1^{WT} and PNRC1^{W300A}, suggesting that PNRC1 RNA-binding capacity is not altered by W300A mutation.

In all, these data suggest that PNRC1 directly binds U3 and U8 snoRNAs likely conferring specificity to DCP2 toward these snoRNAs.

PNRC1^{W300A} mutant does not hinder the enhanced proliferation induced by RAS

We finally asked whether PNRC1 antiproliferative capacity is mediated by its role in restraining rRNA biosynthesis. To this end, we
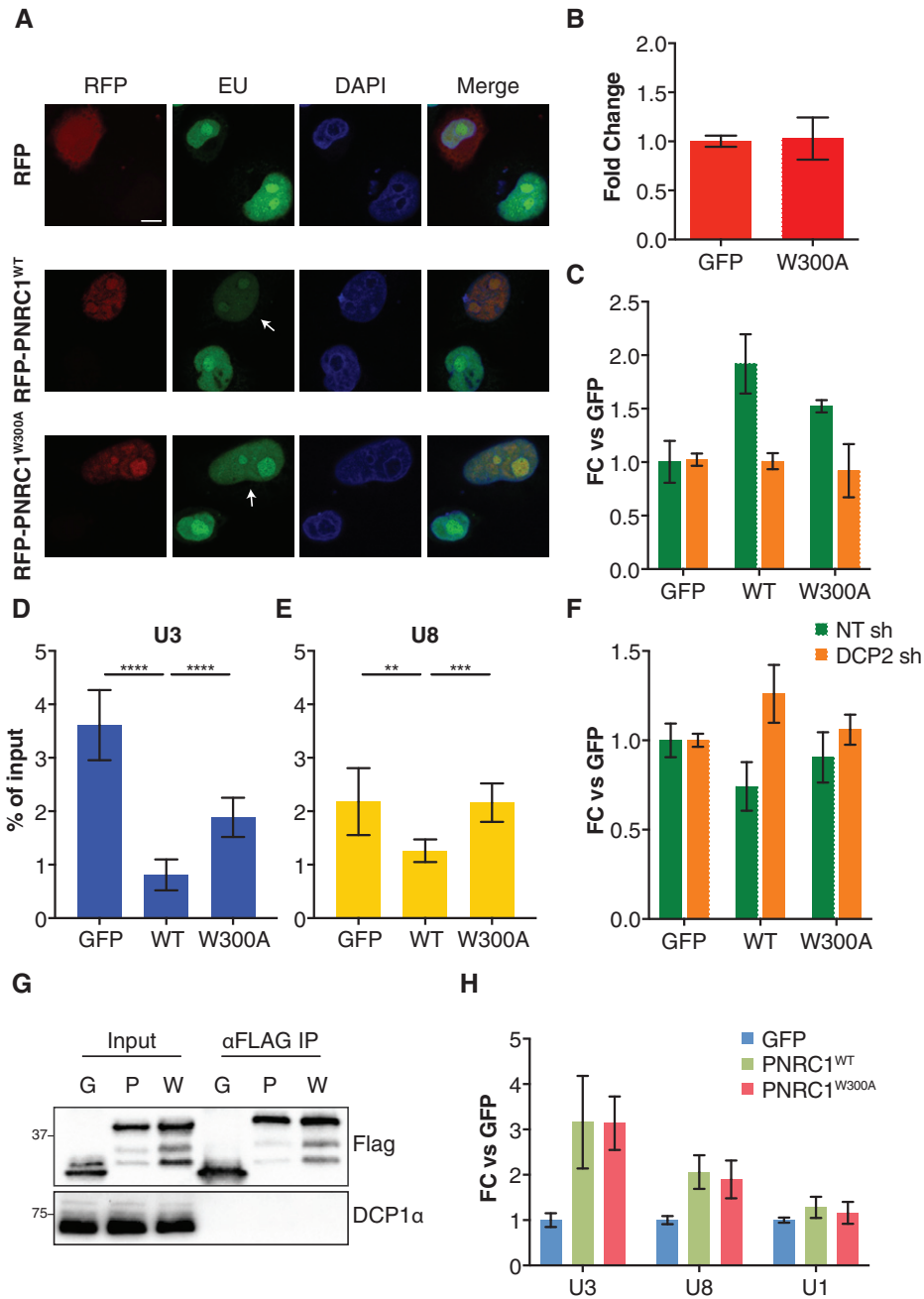
Figure 6. PNRC1 reduces DCP1α-/DCP2-dependent rRNA processing and snoRNA decapping.

A   Confocal images of a Click-iT RNA imaging assay performed on HeLa cells expressing RFP, RFP-PNRC1[WT], or RFP-PNRC1[W300A] pulsed with EU for 16 h and collected after EU removal (green: Alexa 488-EU, red: RFP, blue: DAPI, scale bar: 5 μm). RFP-PNRC1[WT]- or RFP-PNRC1[W300A]-transfected cells are indicated with arrowheads.

B   Real-time PCR quantification of 5′-ETS steady-state levels in HeLa cells expressing PNRC1[W300A] or GFP control. The average of three independent experiments ± SD is reported.

C   Quantification of 5′-ETS RNA levels in HeLa cells infected with an anti-DCP2 or a non-targeting shRNA and expressing GFP, PNRC1[WT], or PNRC1[W300A] transgenes. The average of two independent experiments ± SD is reported.

D, E   Levels of U3 (D) and U8 (E) snoRNAs immunoprecipitated by the anti-m$_3$G cap antibody measured by real-time PCR in HeLa cells infected with GFP, PNRC1[WT], or PNRC1[W300A] transgenes. Values represent the average of two biological replicates with three technical replicates and are expressed as percentages of enrichment compared to the input ± SD. Where indicated, a two-tailed *t*-test was performed combining the technical and biological replicates (****$P < 0.0001$, ***$P < 0.0002$, **$P < 0.002$).

F   Levels of U3 snoRNA immunoprecipitated by the anti-m$_3$G cap antibody in HeLa cells infected with an anti-DCP2 or a non-targeting shRNA and expressing GFP, PNRC1[WT], or PNRC1[W300A] transgenes. The average ± SD of two independent experiments with three technical replicates is reported.

G   Western blot analysis of input and Flag-IP fractions of RNA immunoprecipitation (RIP) experiment performed in HeLa cells infected with GFP control (G), PNRC1[WT] (P) or PNRC1[W300A] (W) transgenes.

H   RNA levels of U3, U8, and U1 co-immunoprecipitating with GFP, PNRC1[WT], or PNRC1[W300A]. Results are shown as the average ± SD of two biological replicates.

performed cell proliferation studies comparing HeLa cells expressing PNRC1[W300A] mutant with PNRC1[WT]-expressing cells (Appendix Fig S1F). PNRC1[WT] hampered proliferation while cells expressing PNRC1[W300A] mutant grew at a similar rate as LacZ control (Fig EV5A). We then evaluated whether PNRC1[W300A] mutant could counteract RAS-driven increased proliferation, as seen with PNRC1[WT]. Cells transfected with both HRAS[G12V] and PNRC1[W300A] (Appendix Fig S1G and H) showed the same proliferation rate as compared to cells expressing HRAS[G12V] alone, unlike PNRC1[WT]-expressing cells that reduced HRAS[G12V]-driven proliferation (Fig EV5B).

Taken together, these results suggest that PNRC1 antiproliferative and tumor-suppressive function relies on the nucleolar recruitment of the cytoplasmic decapping complex and on the consequent block in rRNA biosynthesis.

Discussion

In this study, we have identified a metagene signature that includes a small subset of genes consistently downregulated and hemizygously deleted in several tumor types. These genes are enriched for nucleolar localization. Among them, we have identified PNRC1, up to now classified as a nuclear receptor coactivator. We found that PNRC1 drags the cytoplasmic decapping complex, usually located within the cytoplasm, inside the nucleolus. Here, acting together with several members of the decapping machinery, PNRC1 stimulates U3 and U8 snoRNA decapping, ultimately hampering rRNA maturation (Fig 7, model). As a result, PNRC1 overexpression ablates the enhanced proliferation triggered by established oncogenes such as RAS and MYC. These results suggest that the partial loss of PNRC1 is a pervasive event in carcinogenesis, required to unleash ribosomal synthesis and the translation boost required for oncogenesis.

The two-hit hypothesis by Knudson posits that tumor suppressor genes are lost through genetic or epigenetic events that lead to their biallelic inactivation (Knudson, 1971). More recently, however, a more nuanced perspective has emerged, suggesting that in several cases tumor suppressor genes need not to be completely ablated. This model hypothesizes a sort of dosage-dependency of TSG function (Berger et al, 2011). Recent studies have submitted an even more radical perspective. Large-scale screens based on siRNA have identified putative haploinsufficient tumor suppressor genes that are located within regions of hemizygous deletions. The partial down-regulation of these genes briskly increases cancer cell proliferation, in vitro and in vivo (Greenman, 2012; Xue et al, 2012). However, these screening-based approaches present limitations (Goff, 2008; Mullenders & Bernards, 2009; Miller et al, 2017). To validate and potentially identify additional TSGs, we undertook a complementary strategy, integrating data on copy number and gene expression from TCGA. Starting from the same list of shared deletions, a novel iteration of NMF revealed a metagene signature designated by hemizygous deletions and reduced expression. While STOP genes were enriched in this cluster group, notwithstanding we identified several genes not present in the previous screens, suggesting that these two complementary strategies may provide a more comprehensive annotation of putative TSGs.

One of the most notable findings of our NMF analysis was the identification of the nucleolus as the most enriched GO term within this gene cluster. While the role of the nucleolus and more broadly of processes occurring within this nuclear compartment has long been associated with cancer, the mechanisms underlying the hyper-activation of rDNA transcription have been linked for the most part to the altered activity of specific oncogenes and tumor suppressor genes (Hein et al, 2013). Instead, genetic lesions affecting genes directly related to the nucleolus have been lacking. Based on our findings, we gather that at least a subset of genes directly implicated in nucleolar function are consistently lost and downregulated in several cancer types. One potential implication would be that nucleolar activity is generally tightly controlled in healthy cells. For cancer to ensue, a pervasive loss of these checks needs to emerge, owing to the concomitant loss of several nucleolar genes, dispersed throughout the genome. The finding that the deletions impacting nucleolar genes were for the most part hemizygous is intriguing and suggests that nucleolar proteins are tightly regulated in cancer cells. In fact, the deletions in the 6q15 locus, where PNRC1 resides, are hemizygous in all the tumor types where they have been reported (Johansson et al, 1992; Verhagen et al, 2002; Lapointe et al, 2007; Lee et al, 2008; Remke et al, 2009; Poplawski et al, 2010; Boyd et al, 2012; Lopez-Nieva et al, 2012; Kluth et al, 2013), suggesting that nucleolar genes are likely essential for cell survival. Along this line, we showed that a complete PNRC1 knock-down massively induced apoptosis in HeLa cells, suggesting that the ablation of PNRC1 is lethal for cancer cells (Fig EV2D and E and Appendix Fig S2B). This pattern is reminiscent of ribosomal proteins, whose levels are also tightly controlled. As an example, a recent survey of genomewide shRNA screening data has shown how the reduced expression with shRNAs of hemizygously deleted ribosomal protein genes inhibits cell growth (Ajore et al, 2017). Accordingly, these genes present heterozygous mutations and hemizygous deletions in cancer (Ajore et al, 2017), and in zebrafish, heterozygous mutations of ribosomal genes promote tumorigenesis (Mayer & Grummt, 2006).

Our findings show that the nuclear receptor co-activator PNRC1 interacts with the cytoplasmic 5′–3′ RNA decapping complex and demonstrate that PNRC1 itself is responsible for the translocation of
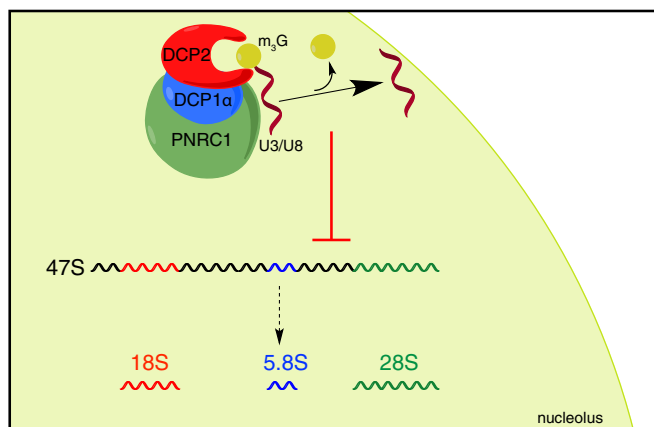

Figure 7. Molecular model for PNRC1-dependent nucleolar RNA decapping.

Schematic model of the molecular events triggered by PNRC1 inside nucleoli. PNRC1 functionally interacts with DCP1α/DCP2 decapping complex acting as a scaffold to tether the decapping machinery inside nucleoli and promoting the m₃G-cap hydrolysis from U3 and U8 snoRNAs, ultimately leading to rRNA processing block.

this molecular machinery inside nucleoli. This is an intriguing finding since the DCP1α/DCP2 complex has long been known to reside within the P-bodies (van Dijk *et al*, 2002; Parker & Sheth, 2007), acting in concert with PNRC2 in the cytoplasmic decay of aberrant mRNAs (Cho *et al*, 2009, 2012, 2013; Lai *et al*, 2012). On the other side, our results may help explain the puzzling interaction that has been reported between PNRC1 and the UPF1 RNA helicase (Cho *et al*, 2009). In agreement with our data, previous observations have shown how cytoplasmic RNA decapping proteins might shuttle between the cytoplasm and the nucleus, where they exert a role in RNA transcription (Brannan *et al*, 2012; Haimovich *et al*, 2013). We now provide first-time evidence that the DCP1α/DCP2 decapping complex localizes also inside nucleoli. Moreover, we show that the nucleolar import of the cytoplasmic RNA decapping machinery has a functional relevance in restraining rRNA processing rates, since it leads to the accumulation of the long polycistronic rRNA precursor and a consequent decrease in mature rRNAs. Indeed, the expression of a mutant form of PNRC1 unable to bind to the DCP1α/DCP2 decapping machinery, as well as the silencing of DCP2 catalytic decapping protein, prevented PNRC1-induced alterations in rRNA processing, demonstrating that PNRC1 requires the presence and the catalytic activity of the decapping complex inside nucleoli to hamper rRNA maturation. Interestingly, enhancers of decapping (like EDC3) involved in RNA polymerase II transcription termination (Brannan *et al*, 2012) are likely dispensable for DCP2 nucleolar activity as EDC3 knock-down did not prevent PNRC1-induced accumulation of rRNA precursors (data not shown).

5′ cap structure is a feature of mRNAs, required for their nuclear export, translation, and stability. On the contrary, rRNAs are generally devoid of cap structures, as both precursors and mature molecules, suggesting that rRNA species might not represent the direct target of PNRC1-organized nucleolar decapping complex. Therefore, it is reasonable to hypothesize that the identified DCP1α-/DCP2-dependent regulation of rRNA maturation governed by PNRC1 might involve other nucleolar RNA species whose decapping ultimately leads to rRNA processing block. Along these lines, modified 5′ cap structures, such as the m_3G tri-methylated cap, are found on nuclear RNA classes different from mRNAs, including some small nucleolar RNAs (Matera *et al*, 2007), whose capping status was shown to be crucial for their stability. Among these, U3 and U8 represent candidate targets for the nucleolar DCP1α/DCP2 complex as they are capped with a m_3G moiety and are required to aid the early cleavage reactions on the 47S rRNA precursor (Peculis & Steitz, 1993; Verheggen *et al*, 2002; Mullineux & Lafontaine, 2012). In line with this hypothesis, we showed that PNRC1 expression is associated with a reduction in the m_3G-capped fraction of both U3 and U8 snoRNAs and we also provided evidence that the DCP1α/DCP2 decapping machinery is involved in this process. These data support the idea that RNA decapping proteins exert broader roles, which go beyond the cytoplasmic degradation of aberrant mRNAs. Along this line, another member of NUDIX hydrolase family, the X29 decapping protein identified in *Xenopus*, was shown to be able to remove the m_3G cap moiety from U8 (Ghosh *et al*, 2004; Peculis *et al*, 2007). Intriguingly, X29 human orthologous NUDT16 maintained the ability to decap U8 snoRNA *in vitro* (Lu *et al*, 2011) but was shown to exert a more prominent effect on cytoplasmic mRNA decapping (Song *et al*, 2010). However, we did not observe any direct interaction of NUTD16 with PNRC1 (Appendix Table S2 and

data not shown), thus indicating that it does not participate in PNRC1-dependent snoRNA decapping.

Our data also show that PNRC1 binds both U3 and U8 snoRNAs and that its interactions with these RNAs are direct as the highly denaturing RIP conditions used in the experiment led to the disruption of protein–protein interactions, as demonstrated by the absence of co-precipitation of DCP1α with PNRC1^{WT} in Fig 6G. These findings are in line with reports showing that decapping accessory proteins contribute to bind DCP1α/DCP2 target RNAs (Deshmukh *et al*, 2008; Arribas-Layton *et al*, 2013; Mugridge *et al*, 2018) and suggest that PNRC1 may act as a molecular platform able to confer substrate specificity to DCP1α/DCP2 complex by keeping the decapping machinery in close proximity to its nucleolar targets.

In all, these data strongly indicate that U3 and U8 snoRNA are candidate targets of the nucleolar decapping machinery ultimately responsible for PNRC1-dependent block in rRNA processing. Curiously, we did not appreciate any significant alteration of total U3 and U8 RNA levels upon PNRC1 expression, despite the pronounced effect on its decapping. This observation suggests that snoRNA 5′ cap may regulate other features of the molecule rather than its stability. Along this line, it was reported that the tri-methylation of U3 and U8 5′ caps is essential for their correct translocation from Cajal bodies to nucleoli (Jacobson & Pederson, 1998; Boulon *et al*, 2004). Stemming from these evidences, we might speculate that the DCP1α/DCP2-dependent decapping may interfere with the correct localization of these snoRNAs inside nucleoli, ultimately reducing their active nucleolar pool involved in rRNA processing.

Our findings also support the view that both members of PNRC protein family may exert a crucial role in driving the activity of the RNA decay complex. Indeed, PNRC1 and PNRC2 show high sequence conservation, including the residues required for DCP1α interaction, but diverge in terms of cellular distribution, as PNRC1 harbors a NLS/NoLS domain that dictates its nucleolar localization (Wang *et al*, 2011). We thus propose that both PNRC1 and PNRC2 act as organizing proteins for the recruitment of the same RNA processing machinery in two different cellular compartments. Nevertheless, while PNRC2 is crucial for the relocation of the hyperphosphorylated UPF1 toward DCP1α already residing in P-bodies (Cho *et al*, 2009), our data suggest that PNRC1 competes with PNRC2, displacing DCP1α and the entire RNA decapping machinery from their canonical P-bodies localization toward the nucleolus. Notwithstanding, there does not seem to be functional redundancy between the two proteins, since forcing PNRC1 in the cytoplasm by deleting its NLS/NoLS domain did not result in its incorporation inside P-bodies. On the contrary, PNRC1^{ΔNLS} mutant showed a diffused cytoplasmic staining and maintained its ability to delocalize DCP1α and the whole decapping machinery from P-bodies (Fig EV5C and D).

Finally, our data suggest that PNRC1 expression is associated with a general reduction in ribosome biogenesis and may account for its tumor-suppressive function. In fact, re-expression of PNRC1 in cancer cell lines with exceedingly low levels of the endogenous protein halts the hyper-proliferative phenotype induced by mutant RAS or MYC oncogenes. Instead, PNRC1^{W300A} is unable to counteract the oncogenic potential of mutated RAS. Therefore, these evidences reinforce the notion that PNRC1-dependent block is an important hurdle that cancer cells need to overcome to unleash their oncogenic proliferative potential.

In conclusion, our results suggest a role for PNRC1 as a gatekeeper tumor suppressor that regulates cell proliferation by tuning the available pool of rRNAs through a novel mechanism acting in concert with the cytoplasmic DCP1α/DCP2 decapping complex that PNRC1 hauls within nucleoli.

Materials and Methods

Non-negative matrix factorization analysis

Data retrieval

Raw segmentation values and RNA-seq median z-scores were downloaded from cBioPortal (Cerami *et al*, 2012), and only tumors, detailed in Appendix Table S3, with both datasets available were considered.

For our analysis, we extracted 2,060 genes annotated by GENCODE v19 (Harrow *et al*, 2012) and included in 81 regions described by Solimini *et al* (2012).

Signature extraction

For each gene–tumor pair, we computed two-dimensional binning of raw CNA values and z-scores, using 16 bins in the range $(-2, 2)$ for CNA and $(-4, 4)$ for RNA. The flat version of such two-dimensional matrices was concatenated in a genewise manner, in order to obtain a $2{,}060 \times 256$ matrix T describing each tumor.

We applied non-negative matrix factorization (Lin, 2007) implemented in scikit-learn v 0.18.1 on each tumor separately; we extracted 10 non-negative components C_T and assigned a gene to a component according to its maximal value in the decomposed matrix.

To aggregate data from different tumors, we calculated pairwise distances among the 280 components using Pearson's r correlation, we clustered data with Ward's method, and finally, we cut the tree at 10 clusters. The average value of components included in a cluster represents a signature. We assigned a gene to a signature by counting the number of occurrences of the appropriate C_T component in each cluster; we assigned a gene to a signature according to the maximal count value.

GO Term Enrichment

Gene Ontology Term Enrichment was performed with Enrichr (Chen *et al*, 2013) using GO Cellular Component 2017 as source of annotation.

Cell culture, transfection, and lentiviral infection

HeLa, MCF7, and HEK293T cells were grown in Dulbecco's Modified Eagle Medium (DMEM, EuroClone), supplemented with 10% heat-inactivated fetal bovine serum (FBS, EuroClone) and 1% Penicillin/Streptomycin (EuroClone). A549 cells were grown in RPMI-1640 medium, supplemented as above. HeLa and MCF7 transient transfections were performed with FuGENE® HD Reagent (Promega), while A549 cells were transfected with JetPRIME® transfection reagent (Polyplus transfections) according to the manufacturers' instructions. For lentivirus production, HEK293T cells were transfected with the calcium phosphate method. To this end, a mix containing 10 μg of transfer vector, 6.5 μg of packaging vector Δr

8.74, 3.5 μg of Env VSV-G, 2.5 μg of REV, ddH$_2$O to 450 μl, 50 μl of 2.5 M CaCl$_2$, and 500 μl of 2× HBS was added dropwise over a monolayer of HEK293T cells seeded on a 10-cm^2 dish. After 16 h, the medium was replaced. Twenty-four hours later, the medium containing virus particles was collected and filtered on a 0.22-μm filter. HeLa cells were infected overday with 2 ml viral medium in 6-well plates and subsequently selected with 1 μg/ml puromycin (Life Technologies) for at least 3 days. Silencing of PNRC1, DCP1α, and DCP2 was obtained through infection of HeLa cells with pLKO.1 lentiviral vectors carrying specific shRNA sequences. The gene-specific constructs derive from the repository generated by Dr. William C. Hahn of Dana-Farber Cancer Institute—The RNAi Consortium (TRC) shRNA Library (https://portals.broadinstitute.org/gpp/public/), while the non-mammalian shRNA control plasmid was purchased from Sigma-Aldrich. The siRNA sequences cloned in pLKO.1 vectors are provided in the Appendix Supplementary Methods section.

Proliferation studies

HeLa, MCF7, and A549 cells were plated in 60-mm dishes and transfected with the indicated constructs as described above. For co-expression studies, equal amounts of the two expression vectors (containing either LacZ or specific ORFs) were transfected simultaneously. Twenty-four hours following transfection, cells were plated in triplicate in 6-well plates (50,000 cells/well for HeLa and A549 cells, 200,000 cells/well for MCF7 cells) with complete medium. Cells were detached and counted in triplicate at the indicated time points with a Bürker cell chamber after Trypan Blue staining to exclude apoptotic/necrotic cells. 0 h time point was counted to confirm an equal number of plated cells, approximately 4 h post-replating. Where indicated, a two-tailed unpaired t-test was applied.

Apoptosis assay

Cell apoptosis was evaluated by flow cytometry taking advantage of the PE Annexin-V Apoptosis Detection Kit (BD Biosciences), according to the manufacturer's protocol. Briefly, cells and cell culture supernatants were harvested, washed twice in calcium- and magnesium-free PBS, and resuspended in binding buffer at the concentration of 10^6 cells/ml. 100 μl of cell suspension was stained with Annexin-V-PE and 7-AAD for 15 min at room temperature, and samples were analyzed by flow cytometry at the Gallios™ (Beckman Coulter). At least 20,000 events per sample were acquired, and percentages of cells positive for Annexin-V and 7-AAD markers were evaluated by analyzing the acquired events with FCS Express 4.0 software (De Novo Software).

Nucleolar fractionation

Nucleolar fractionation protocol was adapted from the method developed in Prof. Lamond's laboratory (http://www.lamondlab.com/newwebsite/Protocols%20for%20Website/Cellular%20Fractionation%20Protocol.pdf). In brief, cytoplasmic fraction was separated from intact nuclei by lysing cells in buffer A (10 mM HEPES pH 7.9, 10 mM NaCl, 1.5 mM MgCl$_2$, 0.1% Triton® X-100, 0.34 M sucrose, 10% glycerol, 1 mM DTT, 1 mM PMSF, 1 mM Na$_3$VO$_4$, 1 mM NaF,

1× Roche Antiproteolytics) and pelleting nuclei by low-speed centrifugation (5 min 1,300 × *g*, 4°C). Nuclei were washed once with buffer A and subsequently resuspended in S2 buffer (0.35 M sucrose, 0.5 mM MgCl$_2$, protease inhibitors as above), 100 μl each 10^6 cells. Nuclei were then sonicated using a Bandelin SONOPULS mini20 sonicator to lyse nuclear membrane and release intact nucleoli (15% power, four cycles, 10 s on/30 s off). The efficiency of nuclear disruption was monitored by light microscopy. Samples were layered over 200 μl S3 buffer (0.88 M sucrose, 0.5 mM MgCl$_2$, protease inhibitors as above) and centrifuged for 10 min at 2,800 × *g*, 4°C. Supernatant corresponding to nucleoplasmic fraction was collected and further clarified by high-speed centrifugation (15 min max speed, 4°C) to remove cell debris and insoluble aggregates. Pelleted nucleoli were washed in S2 buffer, centrifuged (5 min at 2,800 × *g*, 4°C), and lysed in Laemmli + 1× DTT, 100 μl each 10^6 cells. UBF1 was used as nucleolar marker, while PolII was exploited as a marker of a non-nucleolar protein.

rRNA processing assay

To study rRNA maturation, cells were plated on 100-mm dishes and transfected. Twenty-four hours after transfection, cells were detached and seeded in 6-well plates. After 16 h, cell medium was replaced with DMEM supplemented with 3 μCi/ml ^{3}H-uridine (PerkinElmer) and cells were pulsed for 15 min. Where indicated, cells were pre-treated with 5 μM 5-fluorouridine (Sigma-Aldrich) for 15 min to inhibit rRNA processing. Cells were then washed twice with PBS and chased with fresh DMEM for different times. Cells were harvested in TRIzol, and RNA was collected as described in the Appendix Supplementary Methods section. ^{3}H-uridine incorporation in the recovered RNA samples was measured by liquid scintillation using a Tri-Carb B2810TR β-counter (PerkinElmer), and the obtained counts were used to normalize the input RNA amounts. RNA samples were resuspended in denaturing loading buffer (containing 50% formamide and 5% formaldehyde) and heat-denatured at 65°C for 5 min. Samples were loaded on a 1% agarose/formaldehyde denaturing gel and blotted onto a Hybond-N+ nylon membrane (GE Healthcare). RNA was crosslinked to the membrane with UV light using a UV Stratalinker® 2400 crosslinker (Stratagene), and membranes were sprayed with En3Hance™ Spray Surface Autoradiography Enhancer (PerkinElmer) before autoradiography which was performed for 6 days at −80°C.

Immunoprecipitation

HeLa cells were plated on 100-mm dishes (one dish per condition) and transfected as indicated. Twenty-four hours after transfection, cells were washed 2× in PBS and scraped. The pellet was resuspended in IP Lysis Buffer (50 mM HEPES, 150 mM NaCl, 0.1% Tween-20, 1 mM EDTA, 2.5 mM EGTA, 1 mM PMSF, 1 mM Na$_3$VO$_4$, 1 mM NaF, 1× Roche Antiproteolytics), and lysates were sonicated on ice using a Bandelin SONOPULS mini20 sonicator (10 s of 15% amplitude pulse and 30 s of pause for five cycles). Lysates were then clarified by centrifugation for 30 min at max speed (15,000 rpm), 4°C. In the meantime, 80 μl Dynabeads® protein A magnetic beads (Life Technologies) were equilibrated with IP Lysis Buffer. The clarified lysate was then loaded onto 40 μl

beads and pre-cleared for 30 min on a wheel at 4°C. After the preclearing step, the supernatant was recovered and 5% of the supernatant was stored and loaded on a gel as a total input control. The remaining lysate was mixed with 40 μl of the equilibrated beads and with 4 μg of a specific antibody or non-immunized control IgG (Santa Cruz). Tubes were incubated on the wheel overnight at 4°C, and bead supernatants were stored and loaded, where indicated, as unbound fractions. Beads were then washed five times with 500 μl IP Lysis Buffer, and final elution was obtained by resuspending beads with 40 μl of Laemmli 2×. The bead supernatant represents the immunoprecipitated fraction. Where reported, treatment with RNase A (1 mg/ml) was carried out by directly adding the enzyme to cell lysates during overnight incubation with beads and specific antibodies. To verify RNase A efficiency, 5 μl of each unbound fraction was retrotranscribed and GAPDH levels were quantified by real-time PCR as described in the Appendix Supplementary Methods section.

m$_3$G-cap RNA immunoprecipitation was performed according to the protocol published in Jia *et al* (2007). Briefly, 20 μg of total RNA isolated from cells and treated with Turbo DNase (as described in the Appendix Supplementary Methods section) was resuspended in immunoprecipitation buffer supplemented with 300 U/ml RNaseOUT inhibitor (Life Technologies). RNA was pre-cleared with Dynabeads protein G (Life Technologies) for 30′ at 4°C and then incubated overnight with 4 μg of the anti-m$_3$G cap antibody (Santa Cruz Biotechnology) at 4°C with continuous shaking. 2.5% of the pre-cleared RNA was stored as total input. The antibody-bound RNAs were isolated by adding Dynabeads protein G for 2 h at 4°C with continuous shaking, washed, eluted, and extracted as described. Total and immunoprecipitated RNAs were then reverse-transcribed with SuperScript III (Life Technologies) and quantified by real-time PCR.

For RNA immunoprecipitation (RIP), cells expressing Flag-tagged transgenes were exposed to UV-C (150 mJ/cm^2) with a StrataLinker (Stratagene) to promote covalent RNA–protein crosslinking. Cells were lysed in RIP buffer (50 mM Tris/HCl pH 7.4, 100 mM NaCl, 1% NP-40 substitute, 0.1% SDS, 0.5 sodium deoxycholate, 300 U/ml RNase OUT, protease inhibitor), and lysates were cleared by centrifugation. Small lysate aliquots were stored as inputs for both protein and RNA quantifications, while tagged protein–RNA complexes were precipitated overnight at 4°C using anti-Flag M2-coated magnetic beads (Sigma-Aldrich). Beads were washed twice with RIP buffer 300 mM NaCl. One third of the beads were resuspended in Laemmli buffer 2× to elute proteins, and the other fraction was subjected to Turbo DNase treatment (as reported in the Appendix Supplementary Methods section), subsequently washed twice with RIP buffer 300 mM NaCl, 10 mM EDTA and treated with Proteinase K (PK, 5 μg/μl) to elute RNAs. RNA inputs and PK-eluted fractions were purified by TRIzol extraction, and target RNAs were quantified by real-time PCR after reverse transcription.

Expanded View for this article is available online.

Acknowledgements

Author contributions

MG, CV, and GT conceived the study; MG, CV, VP, and GT designed the experiments; MG, CV, and YPS performed the experiments; MG, CV, BMS, MF, SS, and GT analyzed and interpreted the results; DC and GT performed bioinformatical analyses; FI and CD performed the fluorescence experiments on primary samples; AC and AB designed, performed, and analyzed the mass spectrometry experiment. MG and GT wrote the manuscript; MG, VP, DC, and GT revised the manuscript.

Conflict of interest

The authors declare that they have no conflict of interest.

References

Ajore R, Raiser D, McConkey M, Joud M, Boidol B, Mar B, Saksena G, Weinstock DM, Armstrong S, Ellis SR, Ebert BL, Nilsson B (2017) Deletion of ribosomal protein genes is a common vulnerability in human cancer, especially in concert with TP53 mutations. *EMBO Mol Med* 9: 498–507

Arabi A, Rustum C, Hallberg E, Wright AP (2003) Accumulation of c-Myc and proteasomes at the nucleoli of cells containing elevated c-Myc protein levels. *J Cell Sci* 116: 1707–1717

Arribas-Layton M, Wu D, Lykke-Andersen J, Song H (2013) Structural and functional control of the eukaryotic mRNA decapping machinery. *Biochem Biophys Acta* 1829: 580–589

Babu K, Verma R (1985) Structural and functional aspects of nucleolar organizer regions (NORs) of human chromosomes. *Int Rev Cytol* 94: 151–176

Barna M, Pusic A, Zollo O, Costa M, Kondrashov N, Rego E, Rao PH, Ruggero D (2008) Suppression of Myc oncogenic activity by ribosomal protein haploinsufficiency. *Nature* 456: 971–975

Berger AH, Knudson AG, Pandolfi PP (2011) A continuum model for tumour suppression. *Nature* 476: 163–169

Beroukhim R, Mermel CH, Porter D, Wei G, Raychaudhuri S, Donovan J, Barretina J, Boehm JS, Dobson J, Urashima M, Mc Henry KT, Pinchback RM, Ligon AH, Cho YJ, Haery L, Greulich H, Reich M, Winckler W, Lawrence MS, Weir BA *et al* (2010) The landscape of somatic copy-number alteration across human cancers. *Nature* 463: 899–905

Boisvert FM, van Koningsbruggen S, Navascues J, Lamond AI (2007) The multifunctional nucleolus. *Nat Rev Mol Cell Biol* 8: 574–585

Boon K, Caron HN, van Asperen R, Valentijn L, Hermus MC, van Sluis P, Roobeek I, Weis I, Voute PA, Schwab M, Versteeg R (2001) N-myc enhances the expression of a large set of genes functioning in ribosome biogenesis and protein synthesis. *EMBO J* 20: 1383–1393

Boulon S, Verheggen C, Jady BE, Girard C, Pescia C, Paul C, Ospina JK, Kiss T, Matera AG, Bordonne R, Bertrand E (2004) PHAX and CRM1 are required sequentially to transport U3 snoRNA to nucleoli. *Mol Cell* 16: 777–787

Boyd LK, Mao X, Xue L, Lin D, Chaplin T, Kudahetti SC, Stankiewicz E, Yu Y, Beltran L, Shaw G, Hines J, Oliver RT, Berney DM, Young BD, Lu YJ (2012) High-resolution genome-wide copy-number analysis suggests a

monoclonal origin of multifocal prostate cancer. *Genes Chromosom Cancer* 51: 579–589

Brannan K, Kim H, Erickson B, Glover-Cutter K, Kim S, Fong N, Kiemele L, Hansen K, Davis R, Lykke-Andersen J, Bentley DL (2012) mRNA decapping factors and the exonuclease Xrn2 function in widespread premature termination of RNA polymerase II transcription. *Mol Cell* 46: 311–324

Brunet JP, Tamayo P, Golub TR, Mesirov JP (2004) Metagenes and molecular pattern discovery using matrix factorization. *Proc Natl Acad Sci USA* 101: 4164–4169

Carrasco DR, Tonon G, Huang Y, Zhang Y, Sinha R, Feng B, Stewart JP, Zhan F, Khatry D, Protopopova M, Protopopov A, Sukhdeo K, Hanamura I, Stephens O, Barlogie B, Anderson KC, Chin L, Shaughnessy JD Jr, Brennan C, Depinho RA (2006) High-resolution genomic profiles define distinct clinico-pathogenetic subgroups of multiple myeloma patients. *Cancer Cell* 9: 313–325

Cerami E, Gao J, Dogrusoz U, Gross BE, Sumer SO, Aksoy BA, Jacobsen A, Byrne CJ, Heuer ML, Larsson E, Antipin Y, Reva B, Goldberg AP, Sander C, Schultz N (2012) The cBio cancer genomics portal: an open platform for exploring multidimensional cancer genomics data. *Cancer Discov* 2: 401–404

Chan JC, Hannan KM, Riddell K, Ng PY, Peck A, Lee RS, Hung S, Astle MV, Bywater M, Wall M, Poortinga G, Jastrzebski K, Sheppard KE, Hemmings BA, Hall MN, Johnstone RW, McArthur GA, Hannan RD, Pearson RB (2011) AKT promotes rRNA synthesis and cooperates with c-MYC to stimulate ribosome biogenesis in cancer. *Sci Signal* 4: ra56

Chen EY, Tan CM, Kou Y, Duan Q, Wang Z, Meirelles GV, Clark NR, Ma'ayan A (2013) Enrichr: interactive and collaborative HTML5 gene list enrichment analysis tool. *BMC Bioinformatics* 14: 128

Cho H, Kim KM, Kim YK (2009) Human proline-rich nuclear receptor coregulatory protein 2 mediates an interaction between mRNA surveillance machinery and decapping complex. *Mol Cell* 33: 75–86

Cho H, Kim KM, Han S, Choe J, Park SG, Choi SS, Kim YK (2012) Staufen1-mediated mRNA decay functions in adipogenesis. *Mol Cell* 46: 495–506

Cho H, Han S, Choe J, Park SG, Choi SS, Kim YK (2013) SMG5-PNRC2 is functionally dominant compared with SMG5-SMG7 in mammalian nonsense-mediated mRNA decay. *Nucleic Acids Res* 41: 1319–1328

Cho H, Park OH, Park J, Ryu I, Kim J, Ko J, Kim YK (2015) Glucocorticoid receptor interacts with PNRC2 in a ligand-dependent manner to recruit UPF1 for rapid mRNA degradation. *Proc Natl Acad Sci USA* 112: E1540–E1549

Cui C, Tseng H (2004) Estimation of ribosomal RNA transcription rate *in situ*. *Biotechniques* 36: 134–138

Deshmukh MV, Jones BN, Quang-Dang DU, Flinders J, Floor SN, Kim C, Jemielity J, Kalek M, Darzynkiewicz E, Gross JD (2008) mRNA decapping is promoted by an RNA-binding channel in Dcp2. *Mol Cell* 29: 324–336

van Dijk E, Cougot N, Meyer S, Babajko S, Wahle E, Seraphin B (2002) Human Dcp2: a catalytically active mRNA decapping enzyme located in specific cytoplasmic structures. *EMBO J* 21: 6915–6924

Drygin D, Rice WG, Grummt I (2010) The RNA polymerase I transcription machinery: an emerging target for the treatment of cancer. *Annu Rev Pharmacol Toxicol* 50: 131–156

Fayet-Lebaron E, Atzorn V, Henry Y, Kiss T (2009) 18S rRNA processing requires base pairings of snR30 H/ACA snoRNA to eukaryote-specific 18S sequences. *EMBO J* 28: 1260–1270

Ghosh T, Peterson B, Tomasevic N, Peculis BA (2004) *Xenopus* U8 snoRNA binding protein is a conserved nuclear decapping enzyme. *Mol Cell* 13: 817–828

Goff SP (2008) Knockdown screens to knockout HIV-1. *Cell* 135: 417–420

Gomez-Roman N, Grandori C, Eisenman RN, White RJ (2003) Direct activation of RNA polymerase III transcription by c-Myc. *Nature* 421: 290–294

Grandori C, Gomez-Roman N, Felton-Edkins ZA, Ngouenet C, Galloway DA, Eisenman RN, White RJ (2005) c-Myc binds to human ribosomal DNA and stimulates transcription of rRNA genes by RNA polymerase I. *Nat Cell Biol* 7: 311–318

Greenman CD (2012) Cancer. Haploinsufficient gene selection in cancer. *Science* 337: 47–48

Haimovich G, Medina DA, Causse SZ, Garber M, Millan-Zambrano G, Barkai O, Chavez S, Perez-Ortin JE, Darzacq X, Choder M (2013) Gene expression is circular: factors for mRNA degradation also foster mRNA synthesis. *Cell* 153: 1000–1011

Harrow J, Frankish A, Gonzalez JM, Tapanari E, Diekhans M, Kokocinski F, Aken BL, Barrell D, Zadissa A, Searle S, Barnes I, Bignell A, Boychenko V, Hunt T, Kay M, Mukherjee G, Rajan J, Despacio-Reyes G, Saunders G, Steward C *et al* (2012) GENCODE: the reference human genome annotation for The ENCODE Project. *Genome Res* 22: 1760–1774

Hein N, Hannan KM, George AJ, Sanij E, Hannan RD (2013) The nucleolus: an emerging target for cancer therapy. *Trends Mol Med* 19: 643–654

Jacobson MR, Pederson T (1998) A 7-methylguanosine cap commits U3 and U8 small nuclear RNAs to the nucleolar localization pathway. *Nucleic Acids Res* 26: 756–760

Jia D, Cai L, He H, Skogerbo G, Li T, Aftab MN, Chen R (2007) Systematic identification of non-coding RNA 2,2,7-trimethylguanosine cap structures in *Caenorhabditis elegans*. *BMC Mol Biol* 8: 86

Johansson B, Bardi G, Heim S, Mandahl N, Mertens F, Bak-Jensen E, Andren-Sandberg A, Mitelman F (1992) Nonrandom chromosomal rearrangements in pancreatic carcinomas. *Cancer* 69: 1674–1681

Kiss T, Fayet-Lebaron E, Jady BE (2010) Box H/ACA small ribonucleoproteins. *Mol Cell* 37: 597–606

Kluth M, Hesse J, Heinl A, Krohn A, Steurer S, Sirma H, Simon R, Mayer PS, Schumacher U, Grupp K, Izbicki JR, Pantel K, Dikomey E, Korbel JO, Plass C, Sauter G, Schlomm T, Minner S (2013) Genomic deletion of MAP3K7 at 6q12-22 is associated with early PSA recurrence in prostate cancer and absence of TMPRSS2:ERG fusions. *Mod Pathol* 26: 975–983

Knudson AG Jr (1971) Mutation and cancer: statistical study of retinoblastoma. *Proc Natl Acad Sci USA* 68: 820–823

Lai T, Cho H, Liu Z, Bowler MW, Piao S, Parker R, Kim YK, Song H (2012) Structural basis of the PNRC2-mediated link between mRNA surveillance and decapping. *Structure* 20: 2025–2037

Lapointe J, Li C, Giacomini CP, Salari K, Huang S, Wang P, Ferrari M, Hernandez-Boussard T, Brooks JD, Pollack JR (2007) Genomic profiling reveals alternative genetic pathways of prostate tumorigenesis. *Can Res* 67: 8504–8510

Lee SA, Ho C, Roy R, Kosinski C, Patil MA, Tward AD, Fridlyand J, Chen X (2008) Integration of genomic analysis and *in vivo* transfection to identify sprouty 2 as a candidate tumor suppressor in liver cancer. *Hepatology* 47: 1200–1210

Lin CJ (2007) Projected gradient methods for nonnegative matrix factorization. *Neural Comput* 19: 2756–2779

Lopez-Nieva P, Vaquero C, Fernandez-Navarro P, Gonzalez-Sanchez L, Villa-Morales M, Santos J, Esteller M, Fernandez-Piqueras J (2012) EPHA7, a new target gene for 6q deletion in T-cell lymphoblastic lymphomas. *Carcinogenesis* 33: 452–458

Lu G, Zhang J, Li Y, Li Z, Zhang N, Xu X, Wang T, Guan Z, Gao GF, Yan J (2011) hNUDT16: a universal decapping enzyme for small nucleolar RNA and cytoplasmic mRNA. *Protein Cell* 2: 64–73

Ma H, Pederson T (2008) Nucleophosmin is a binding partner of nucleostemin in human osteosarcoma cells. *Mol Biol Cell* 19: 2870–2875

Marmier-Gourrier N, Clery A, Schlotter F, Senty-Segault V, Branlant C (2011) A second base pair interaction between U3 small nucleolar RNA and the

5′-ETS region is required for early cleavage of the yeast pre-ribosomal RNA. *Nucleic Acids Res* 39: 9731–9745

Matera AG, Terns RM, Terns MP (2007) Non-coding RNAs: lessons from the small nuclear and small nucleolar RNAs. *Nat Rev Mol Cell Biol* 8: 209–220

Mayer C, Grummt I (2006) Ribosome biogenesis and cell growth: mTOR coordinates transcription by all three classes of nuclear RNA polymerases. *Oncogene* 25: 6384–6391

Miller TE, Liau BB, Wallace LC, Morton AR, Xie Q, Dixit D, Factor DC, Kim LJY, Morrow JJ, Wu Q, Mack SC, Hubert CG, Gillespie SM, Flavahan WA, Hoffmann T, Thummalapalli R, Hemann MT, Paddison PJ, Horbinski CM, Zuber J *et al* (2017) Transcription elongation factors represent *in vivo* cancer dependencies in glioblastoma. *Nature* 547: 355–359

Moss T, Langlois F, Gagnon-Kugler T, Stefanovsky V (2007) A housekeeper with power of attorney: the rRNA genes in ribosome biogenesis. *Cell Mol Life Sci* 64: 29–49

Mugridge JS, Tibble RW, Ziemniak M, Jemielity J, Gross JD (2018) Structure of the activated Edc1-Dcp1-Dcp2-Edc3 mRNA decapping complex with substrate analog poised for catalysis. *Nat Commun* 9: 1152

Mullenders J, Bernards R (2009) Loss-of-function genetic screens as a tool to improve the diagnosis and treatment of cancer. *Oncogene* 28: 4409–4420

Mullineux ST, Lafontaine DL (2012) Mapping the cleavage sites on mammalian pre-rRNAs: where do we stand? *Biochimie* 94: 1521–1532

Nijhawan D, Zack TI, Ren Y, Strickland MR, Lamothe R, Schumacher SE, Tsherniak A, Besche HC, Rosenbluh J, Shehata S, Cowley GS, Weir BA, Goldberg AL, Mesirov JP, Root DE, Bhatia SN, Beroukhim R, Hahn WC (2012) Cancer vulnerabilities unveiled by genomic loss. *Cell* 150: 842–854

Parker R, Sheth U (2007) P bodies and the control of mRNA translation and degradation. *Mol Cell* 25: 635–646

Peculis BA, Steitz JA (1993) Disruption of U8 nucleolar snRNA inhibits 5.8S and 28S rRNA processing in the *Xenopus* oocyte. *Cell* 73: 1233–1245

Peculis BA, Steitz JA (1994) Sequence and structural elements critical for U8 snRNP function in *Xenopus* oocytes are evolutionarily conserved. *Genes Dev* 8: 2241–2255

Peculis BA (1997) The sequence of the 5′end of the U8 small nucleolar RNA is critical for 5.8 S and 28S rRNA maturation. *Mol Cell Biol* 17: 3702–3713

Peculis BA, Reynolds K, Cleland M (2007) Metal determines efficiency and substrate specificity of the nuclear NUDIX decapping proteins X29 and H29K (Nudt16). *J Biol Chem* 282: 24792–24805

Perez-Fernandez J, Martin-Marcos P, Dosil M (2011) Elucidation of the assembly events required for the recruitment of Utp 20, Imp4 and Bms1 onto nascent pre-ribosomes. *Nucleic Acids Res* 39: 8105–8121

Pianese G (1896) *Beitrag zur histologie und aetiologie des carcinoms*. Jena: G. Fischer

Poplawski AB, Jankowski M, Erickson SW, Diaz de Stahl T, Partridge EC, Crasto C, Guo J, Gibson J, Menzel U, Bruder CE, Kaczmarczyk A, Benetkiewicz M, Andersson R, Sandgren J, Zegarska B, Bala D, Srutek E, Allison DB, Piotrowski A, Zegarski W *et al* (2010) Frequent genetic differences between matched primary and metastatic breast cancer provide an approach to identification of biomarkers for disease progression. *Eur J Hum Genet* 18: 560–568

Preti M, O'Donohue MF, Montel-Lehry N, Bortolin-Cavaille ML, Choesmel V, Gleizes PE (2013) Gradual processing of the ITS1 from the nucleolus to the cytoplasm during synthesis of the human 18S rRNA. *Nucleic Acids Res* 41: 4709–4723

Raska I (2003) Oldies but goldies: searching for Christmas trees within the nucleolar architecture. *Trends Cell Biol* 13: 517–525

Remke M, Pfister S, Kox C, Toedt G, Becker N, Benner A, Werft W, Breit S, Liu S, Engel F, Wittmann A, Zimmermann M, Stanulla M, Schrappe M, Ludwig WD, Bartram CR, Radlwimmer B, Muckenthaler MU, Lichter P, Kulozik AE (2009) High-resolution genomic profiling of childhood T-ALL reveals

frequent copy-number alterations affecting the TGF-beta and PI3K-AKT pathways and deletions at 6q15-16.1 as a genomic marker for unfavorable early treatment response. *Blood* 114: 1053−1062

Riba M, Garcia Manteiga JM, Bosnjak B, Cittaro D, Mikolka P, Le C, Epstein MM, Stupka E (2016) Revealing the acute asthma ignorome: characterization and validation of uninvestigated gene networks. *Sci Rep* 6: 24647

Schlosser I, Holzel M, Murnseer M, Burtscher H, Weidle UH, Eick D (2003) A role for c-Myc in the regulation of ribosomal RNA processing. *Nucleic Acids Res* 31: 6148−6156

Sloan KE, Mattijssen S, Lebaron S, Tollervey D, Pruijn GJ, Watkins NJ (2013) Both endonucleolytic and exonucleolytic cleavage mediate ITS1 removal during human ribosomal RNA processing. *J Cell Biol* 200: 577−588

Solimini NL, Xu Q, Mermel CH, Liang AC, Schlabach MR, Luo J, Burrows AE, Anselmo AN, Bredemeyer AL, Li MZ, Beroukhim R, Meyerson M, Elledge SJ (2012) Recurrent hemizygous deletions in cancers may optimize proliferative potential. *Science* 337: 104−109

Solimini NL, Liang AC, Xu C, Pavlova NN, Xu Q, Davoli T, Li MZ, Wong KK, Elledge SJ (2013) STOP gene Phactr4 is a tumor suppressor. *Proc Natl Acad Sci USA* 110: E407−E414

Song MG, Li Y, Kiledjian M (2010) Multiple mRNA decapping enzymes in mammalian cells. *Mol Cell* 40: 423−432

Sylvester JE, Gonzalez IL, Mougey EB (2004) Structure and organization of vertebrate ribosomal DNA. In *The nucleolus*, Olson MO (ed.), pp 58−72. NewYork, NY: Kluwer Academic/Plenum

Tritschler F, Braun JE, Motz C, Igreja C, Haas G, Truffault V, Izaurralde E, Weichenrieder O (2009) DCP1 forms asymmetric trimers to assemble into active mRNA decapping complexes in metazoa. *Proc Natl Acad Sci USA* 106: 21591−21596

Verhagen PC, Hermans KG, Brok MO, van Weerden WM, Tilanus MG, de Weger RA, Boon TA, Trapman J (2002) Deletion of chromosomal region 6q14-16 in prostate cancer. *Int J Cancer* 102: 142−147

Verheggen C, Lafontaine DL, Samarsky D, Mouaikel J, Blanchard JM, Bordonne R, Bertrand E (2002) Mammalian and yeast U3 snoRNPs are matured in specific and related nuclear compartments. *EMBO J* 21: 2736−2745

Wadi L, Meyer M, Weiser J, Stein LD, Reimand J (2016) Impact of outdated gene annotations on pathway enrichment analysis. *Nat Methods* 13: 705−706

Wang Y, Chen B, Li Y, Zhou D, Chen S (2011) PNRC accumulates in the nucleolus by interaction with B23/nucleophosmin via its nucleolar localization sequence. *Biochem Biophys Acta* 1813: 109−119

Wilkinson DS, Tlsty TD, Hanas RJ (1975) The inhibition of ribosomal RNA synthesis and maturation in Novikoff hepatoma cells by 5-fluorouridine. *Can Res* 35: 3014−3020

Xue W, Kitzing T, Roessler S, Zuber J, Krasnitz A, Schultz N, Revill K, Weissmueller S, Rappaport AR, Simon J, Zhang J, Luo W, Hicks J, Zender L, Wang XW, Powers S, Wigler M, Lowe SW (2012) A cluster of cooperating tumor-suppressor gene candidates in chromosomal deletions. *Proc Natl Acad Sci USA* 109: 8212−8217

Zhao J, Yuan X, Frodin M, Grummt I (2003) ERK-dependent phosphorylation of the transcription initiation factor TIF-IA is required for RNA polymerase I transcription and cell growth. *Mol Cell* 11: 405−413

Zhou D, Quach KM, Yang C, Lee SY, Pohajdak B, Chen S (2000) PNRC: a proline-rich nuclear receptor coregulatory protein that modulates transcriptional activation of multiple nuclear receptors including orphan receptors SF1 (steroidogenic factor 1) and ERRalpha1 (estrogen related receptor alpha-1). *Mol Endocrinol* 14: 986−998

Zhou D, Chen B, Ye JJ, Chen S (2004) A novel crosstalk mechanism between nuclear receptor-mediated and growth factor/Ras-mediated pathways through PNRC-Grb2 interaction. *Oncogene* 23: 5394−5404

Zhou D, Zhong S, Ye JJ, Quach KM, Johnson DL, Chen S (2007) PNRC is a unique nuclear receptor coactivator that stimulates RNA polymerase III-dependent transcription. *J Mol Signaling* 2: 5